UNIVERSITÀ DEGLI STUDI DI MILANO

Facoltà di Scienze e Tecnologie
Laurea Magistrale in Fisica

Odd Elasticity and Topological Flexural Waves in Active Plates

Relatore Interno: **Prof. Luca Guido Molinari**
Relatore Esterno: **Prof. Vincenzo Vitelli**

Elaborato finale di:
Michele Fossati
Matricola n° 957552
A.A. 2020/2021

Contents

Introduction

Active matter regards a variety of out-of-equilibrium systems in which the individual units are subjected to a continuous injection of energy in order to execute self-sustained motion or work [1, 2]. Examples of such systems typically come from biology, with populations of bacteria or cytoskeletal filaments, or may involve robotic ensembles. In these cases, chemical or electric energy is used by the active units to perform local movements, deformations, orientation arrangements leading to collective flocking, synchronization or pattern formation [3–6]. Active systems can constitute new kinds of materials, which can be studied with the tools of condensed matter and statistical mechanics; the goal is both to understand quantitatively the behaviour of biological systems and to design new synthetic materials able to show phenomena inaccessible to passive matter [7]. In fact, with the injection of energy it is possible to break fundamental and commonly-shared properties as spatiotemporal symmetries [8–10] as well as reciprocity relations [6, 11].

This thesis consist in a development of the continuum theory for active elasticity called *odd elasticity*. Such theory has been recently proposed in [12] and consists in the classical theory of linear elasticity, enlarged with the possibility for the system to exert non-conservative internal stresses and thus to violate the conservation of energy. In fact, an active system in which energy is injected by internal or external local resources, effectively does not conserve energy, when the resources are integrated out. This condition has repercussions on the structure of the elastic tensor—which relates the deformation of the medium to the elastic stresses generated in response—and allows a new anti-symmetric part of the elastic tensor; hence, the name of the theory. Typical odd-elastic signatures consist in the existence of cycles of deformation under which the internal non-conservative forces exert a finite amount of work, together with wave propagation in strong drag regimes, sustained by the energy extracted along the cycles.

Odd elasticity has recently been observed in mechanical and biological systems. In [13], the elastic response of a metallic beam is enriched by mounting a series of piezoelectric sensors and actuators. When the beam is deformed, each sensors produces an electric impulse, which is modified through an external electric circuit and sent to the adjacent actuator. In this way, energy can be injected in the system by the external circuit, keeping the response local and proportional to the deformation—as required by linear elasticity. A biological example is [14], in

which a self-organized crystal of swimming starfish embryos shows self-sustained oscillations, as predicted by the odd-elastic model.

The theory of odd elasticity has been developed for flat 2D and 3D solids [12] (in 1D the elastic tensor is necessarily symmetric), leaving a gap for plates and shells: thin three-dimensional systems, nearly two-dimensional. These shapes can model biological membranes, such as cell cortex and epithelial tissues, and they are also typical structural elements for engineered systems. In this work we study the archetypal and simplest case of a flat plate of finite, small, thickness. An important reference in the literature is [9], where a full covariant theory for the elasticity of active shells of arbitrary shape is constructed. That theory is more general than ours in considering arbitrary shapes and not only flat plates; however, as explained in Appendix B of [9], the authors assume that "the points along the normal to the initial surface before deformation are along the normal to the new surface after deformation". This restrictive assumption will not be applied here, allowing the point along the normal to the initial surface to be reoriented after the deformation. As we will see, it will be a crucial difference, necessary for the results obtained on the flexural (bending) waves.

In this thesis we derive the equations of motion for an odd elastic plate and study the structure of the non-conservative cycles of deformations. We then focus on the bending dynamics. We find that, when the active elastic moduli are dominant over the passive ones, the normal modes' bands become gapped. This allows for the definition of a topological invariant for each band, the Chern number. We analytically compute the Chern number and identify a non-trivial topological structure of the bulk normal modes. This is related to the existence of exotic *edge modes* at the boundary of the system or at interfaces by the principle of *bulk-edge correspondence*. The edge modes propagate unidirectionally along the boundaries, without backscattering against defects or obstructions.

Our system can then be considered a classical analogue of what in quantum condensed matter is called *topological insulator*. These systems have an insulating bulk (because they have the Fermi energy in a band-gap) but host conducting edge states at the boundaries or at interfaces [15]. Classical analogues of topological insulators were recently discovered, with realizations that span from photonics [16] to acoustic waves [17] and mechanical isostatic lattices [18]. Moreover, classical topological insulators have been proposed and realized exploiting the effects of activity; employing self-propelled particles confined to flow in lattices of connected annuli [19] or onto curved surfaces [20]. Another interesting class of systems that show topological protection are those fluids which display a dissipationless transverse viscosity, called *odd viscosity* [21]; these comprehend both passive rotating fluids subjected to Coriolis force [22] both active fluids composed by self-spinning particles [10].

In the last part of the work, we show that under some circumstances our system can be exactly mapped on an odd-viscous fluid. This allows us to visualize the edge modes, re-adapting the simulations made for the fluid system in [21].

The work is structured as follows. In the first chapter we review linear elasticity and present odd elasticity, discussing the symmetry implications and introducing its fundamental features: non-conservative work cycles and active wave propagation in strong drag regimes. The second chapter is devoted to topological insulators; we review the mathematical tools necessary for the definition of the Chern number and show its usage in the study of band structures. We also present the edge modes and the principle of bulk-edge correspondence. In the third chapter we set up our model for the odd-elastic plate; we derive the constitutive relations, together with the equations of motion and discuss the active work-cycles. In the fourth chapter we study the topological properties of the flexural dynamics; we show the opening of the gap for increasing activity and analytically compute the Chern number in a restricted case. We then show the exact mapping on odd-viscous fluids and discuss the existence of edge modes.

Chapter 1

Odd elasticity

Odd elasticity is the linear elastic theory of active solids that exert non conservative forces as a response to deformations [12]. A material is said to be active if its unit components are capable of injecting energy into the system, so that the coarse-grained dynamics effectively does not conserve energy. The mechanical properties of a linear elastic system are encoded in the elastic tensor, which expresses the internal stress as a linear function of the strain tensor. The absence of a conserved energy comes together with a non-zero anti-symmetric part of the elastic tensor, otherwise prohibited. Odd elastic systems allow for the extraction of energy when subjected to quasistatic deformation cycles. Dynamically, the energy extracted from the cycles can be used for the propagation of active waves in strong drag regimes.

In the first section we review the theory of linear elasticity, also called Cauchy elasticity, which describes solids in the continuum. We introduce the strain tensor, which describes the deformations of the elastic medium, and the stress tensor, which describes the elastic internal forces. We then introduce the elastic tensor as a linear map between the strain and the stress and declare the equations of motion. In the second section we see how symmetries and affect the structure of the elastic tensor. Odd elasticity is introduced as an antisymmetric contribution to the elastic tensor, equivalent to a violation of the conservation of energy. In the third section we discuss the compatibility of odd elasticity with the other symmetries. We show that in three dimension odd elasticity is not compatible with isotropy, whereas it is compatible if we only require isotropy with respect to a fixed axis (cylindrical isotropy). We then derive the most general cylindrically isotropic elastic tensor . Later, we write the equations of motion for the elastic medium. In the fourth section we show that the elastic tensor of a non-conservative system has an anti-symmetric (odd) component. The coefficients of the anti-symmetric part, the odd moduli, are directly related to the work that can be extracted deforming the elastic medium in a cyclic way, due to the non-conservativity of the internal forces. In the fifth section we discuss the effects of odd elasticity in the dynamics, showing that it allows the propagation of waves in the overdamped regime, differenlty from passive

systems.

1.1 Linear elasticity

1.1.1 Displacement field

Consider a continuum system that undergoes a small deformation. Let us call $\mathbf{x}$ the position of a point of an elastic medium, with Cartesian components x_i, may it be two or three dimensional. The deformation performs the transformation $\mathbf{x} \mapsto \mathbf{x'}$. The *displacement field* of the deformation is the vector field defined over the system at rest, that in each point gives the amount of displacement undergone by the point [23]

$$\boldsymbol{\xi}(\mathbf{x}) = \mathbf{x'} - \mathbf{x}. \tag{1.1}$$

1.1.2 Strain tensor

A common assumption is that an elastic response follows a change of the internal distances of the system. For instance, a rigid translation, described by an uniform displacement field, does not cause any elastic behaviour.

Consider two near points $\mathbf{x}$ and $\mathbf{x} + \mathbf{dx}$. Their distance is $dl = |\mathbf{dx}|$. The deformation maps

$$\begin{aligned} \mathbf{x} &\mapsto \mathbf{x} + \boldsymbol{\xi}(\mathbf{x}) \\ \mathbf{x} + \mathbf{dx} &\mapsto \mathbf{x} + \mathbf{dx} + \boldsymbol{\xi}(\mathbf{x} + \mathbf{dx}). \end{aligned} \tag{1.2}$$

The distance after the deformation is

$$dl'^2 = |\mathbf{dx} + \boldsymbol{\xi}(\mathbf{x} + \mathbf{dx}) - \boldsymbol{\xi}(\mathbf{x})|^2. \tag{1.3}$$

Expanding the displacement field in $\mathbf{x}$, at the first order we get

$$\begin{aligned} dl'^2 &= (dx_i + \partial_j \xi_i dx_j)(dx_i + \partial_k \xi_j dx_k) \\ &= dl^2 + 2\partial_i \xi_j dx_i dx_j + \partial_i \xi_k \partial_j \xi_k dx_i dx_j. \end{aligned} \tag{1.4}$$

Then, noting that the indices ij are symmetrized by the contraction with $dx_i dx_j$, it can be rewritten as

$$dl'^2 = dl^2 + 2u_{ij} dx_i dx_i = (\delta_{ij} + 2\varepsilon_{ij}) dx_i dx_j \tag{1.5}$$

where ε_{ij} is the *strain tensor* defined by

$$\varepsilon_{ij} = \frac{1}{2} \left(\partial_i \xi_j + \partial_j \xi_i + \partial_i \xi_k \partial_j \xi_k \right). \tag{1.6}$$

The strain tensor captures the variation of the metric tensor under a displacement and in fact it is symmetric by construction. It depends only on the derivatives of the displacement field, reflecting the fact that rigid translations do not change internal distances. If we consider small deformations, i.e. a weakly

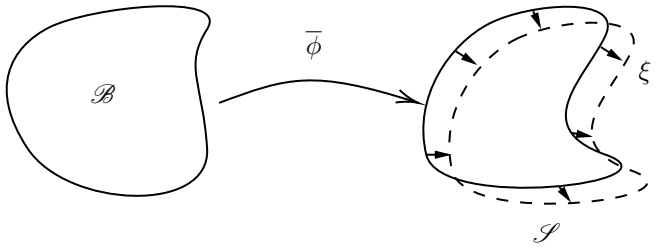

Figure 1.1: An element ξ of the tangent space of $\bar{\phi}$ describes a vector field on $\bar{\phi}(\mathscr{B})$.

varying displacement field, we are justified to neglect the nonlinear terms in Eq. 1.6, obtaining the *linear strain tensor*

$$u_{ij} = \partial_{(i}\xi_{j)}, \tag{1.7}$$

where the round brackets indicate the symmetrization of the indices. In this work we keep ourselves within the framework of linear elasticity, thus will employ only the linear strain tensor. We will call the linear strain tensor just "strain tensor", for simplicity. We note that a rigid rotation, described by a vector field that has a uniform antisymmetric gradient, has zero strain. This is as expected, as rotations do not change internal distances.

1.1.3 A mathematical note

We would like to make a clarification on the mathematical structure of linear elasticity and in particular on the "essence" of the displacement field.

In the mathematical literature [24], a *simple body* $\mathscr{B}$ is a sub-manifold of $\mathbb{R}^3$ and a *configuration* of the body is a regular map ϕ from $\mathscr{B}$ to the space in which the body moves $\mathscr{S}$, thus $\phi : \mathscr{B} \to \mathscr{S}$, where typically $\mathscr{S} = \mathbb{R}^3$. A *motion* is time-dependent family of configurations ϕ_t and it is the unknown variable of the equations of motion. We denote the space of configurations, the set of regular maps from $\mathscr{B}$ to $\mathscr{S}$, with $\mathscr{C}$. It is a function space with the structure of an infinite-dimensional manifold. A motion then describes a curve on $\mathscr{C}$.

The linearized equations of motion around a reference configuration $\bar{\phi}$ will be equations for a curve $\xi(t)$ in the tangent space of the manifold $\mathscr{C}$ at point $\bar{\phi}$. This vector represents the direction of an infinitesimal variation of the reference configuration. By looking at Fig. 1.1, we can convince ourselves that such a vector ξ (which lives in the tangent space of a function space) actually describes a vector field that covers $\bar{\phi}(\mathscr{B})$. This is precisely the vector field that enters in the equations of linear elasticity. We call it the *generator* $\boldsymbol{\xi}$ *of the deformation.*

We now assume the ambient space $\mathscr{S}$ to be $\mathbb{R}^3$ and choose the reference configuration $\bar{\phi} = \mathrm{id}_{\mathscr{B}}$. We consider a curve $\epsilon \mapsto \phi_\epsilon \ni \mathscr{C}$ such that $\phi_0 = \mathrm{id}_{\mathscr{B}}$ and expand it powers of ϵ:

$$\phi_\epsilon(\mathbf{x}) = \mathbf{x}' = \mathbf{x} + \epsilon\boldsymbol{\xi}(\mathbf{x}) + \mathcal{O}(\epsilon^2), \tag{1.8}$$

where

$$\boldsymbol{\xi}(\mathbf{x}) = \frac{d}{d\epsilon}\phi_\epsilon(\mathbf{x})\bigg|_{\epsilon=0}. \tag{1.9}$$

The generator is *tangent* to the displacement and not a displacement itself. It is the direction of an infinitesimal displacement but it can represent a finite displacement if we make use (as we silently do) of the *exponential map*. This means that we identify a vector field with its integral flow, evaluated when the parameter of the flow is equal to one. Concretely, the transformation associated to the vector $\boldsymbol{\xi}$ is $\phi_{\epsilon=1}$. Then, looking at (1.8), we see that if the high order terms are negligible, for $\epsilon = 1$ we get

$$\mathbf{x}' - \mathbf{x} \simeq \boldsymbol{\xi}(\mathbf{x}) \tag{1.10}$$

and regain the classical definition of the displacement field (1.1). We stress that the classical definition of the displacement field is imprecise and that the equations of linear elasticity regard the generator of the deformation, as shown in Marsden's book [24]. The distinction between $\boldsymbol{\xi}(\mathbf{x})$ and $\mathbf{x}' - \mathbf{x}$ becomes relevant when the high order terms in ϵ are not negligible.

When are we allowed to drop those high order terms? Recall that, using the exponential map, the flow is evaluated at $\epsilon = 1$. The second order term of (1.8) is

$$\frac{1}{2}\frac{d^2}{d\epsilon^2}\Phi_\epsilon(\mathbf{x})\bigg|_{\epsilon=0},$$

which is a second derivative of the flow and a first derivative of the generator $\boldsymbol{\xi}$. Thus, if the generator is slowly varying, the physical displacement $\mathbf{x}' - \mathbf{x}$ is well approximated by the vector $\boldsymbol{\xi}(\mathbf{x})$, otherwise it may be something different.

Example: rotations

An instructive example is with rotations. Suppose that the body undergoes a rigid rotation along an axis $\hat{n}$ by an angle θ. The deformation $\mathbf{x} \mapsto \mathbf{x}'$ expressed in Cartesian coordinates is

$$x_i' = R(\hat{n}, \theta)_{ij} x_j. \tag{1.11}$$

Here $R(\hat{n}, \theta) = \exp\big(\theta n_k J^{(k)}\big)$ is a rotation matrix and $J^{(k)}$ are the generators of rotations (antisymmetric matrices). The rotation is already expressed as a flow, it is then straightforward to show that the generator of $R(\hat{n}, \theta)$ is

$$\xi_i(\mathbf{x}) = \theta n_k J^{(k)}_{ij} x_j. \tag{1.12}$$

This quantity is different from

$$\begin{aligned} x'_i - x_i &= R(\hat{n},\theta)_{ij}x_j - x_i \\ &= \sum_{m=0}^{\infty} \frac{\theta^m \left[\left(n_k J^{(k)}\right)^m\right]_{ij}}{m!} x_j - x_i \\ &= \sum_{m=1}^{\infty} \frac{\theta^m \left[\left(n_k J^{(k)}\right)^m\right]_{ij}}{m!} x_j \end{aligned} \tag{1.13}$$

as long as θ is finite. The two quantities match in the limit $\theta \to 0$.

If we then calculate the gradient of the generator $\partial_i \xi_j$, we recover exactly the anti-symmetric matrix that generates the rotation

$$\partial_i \xi_j = \theta n_k J^{(k)}_{ij}. \tag{1.14}$$

More generally, for any displacement field $\boldsymbol{\xi}$ with form

$$\xi_i(\mathbf{x}) = N_{ij}x_j \tag{1.15}$$

the integral curve $\mathbf{x}(\lambda)$ must satisfy:

$$\frac{d}{d\lambda}x_i = \xi_i(\mathbf{x}) = N_{ij}x_j \tag{1.16}$$

which means that $x_i(\lambda) = \exp(\lambda N)_{ij}x_j$ and

$$x'_i = \exp(N)_{ij}x_j. \tag{1.17}$$

Finally, we have shown that the physical displacement $\mathbf{x}' - \mathbf{x}$ and the generator $\boldsymbol{\xi}$ are in general two different objects, related by the exponential map. These tend to coincide if the generator is spatially slowly varying. If the deformation is a linear map that acts on the coordinates with a matrix multiplication, the gradient of the generator field generates the required matrix via an exponential. As the matrix generators of rotations are antisymmetric matrices, we have learnt that the transformation associated to a displacement field whose gradient is a uniform antisymmetric matrix is a rigid rotation.

A geometric construction for the strain tensor

We have already said that the strain tensor describes the variation of internal distances. Distances are measured with the Euclidean metric, thus the variation of distances is quantified by the variation of the Euclidean metric under the deformation. In order to compare the metric before and after the deformation, we have to compare the Euclidean metric g with its pullback through the flow $\phi^*_\epsilon g$. The strain tensor is then defined as infinitesimal variation of the metric under the flow.

$$2u = \lim_{\epsilon\to 0} \frac{\phi^*_\epsilon g - g}{\epsilon} = \frac{d}{d\epsilon}\phi^*_\epsilon g\Big|_{\epsilon=0}. \tag{1.18}$$

It can be shown that the right and side is precisely the *Lie derivative* of the metric in the direction of $\boldsymbol{\xi}$: $2u = \pounds_\xi g$. Assuming that the covariant derivative is compatible with the metric, the Lie derivative of the metric (and thus, the strain) can be expressed as

$$u_{ij} = \frac{1}{2}(\nabla_i \xi_j + \nabla_j \xi_i). \tag{1.19}$$

This allows us to compute the strain tensor in arbitrary coordinates (for instance, polar coordinates).

1.1.4 Stress tensor

The internal forces that give rise to an elastic behaviour are described by the stress tensor. The range of the internal elastic forces is of the order of the intra-molecular distance, thus at the scales of the continuum theory it can be considered a zero range interaction. This implies that if we consider two adjacent portions of the medium, their interaction involves only the contact surface. Such forces are indeed called contact forces or surface forces. The total force exerted on a portion A of the system is given by the sum of the forces exerted on all the volume elements in the portion

$$F_i = \int_A d^3x \, f_i. \tag{1.20}$$

But we know that the forces between the volume elements cancel each other because of Newton's third law. Hence, the total force on the portion is given by the forces exerted by the surrounding portions. The total force can be written as a surface integral, implying that the force field is the divergence of a rank two tensor, the *stress tensor*

$$f_i = \partial_j \sigma_{ij}. \tag{1.21}$$

The surface integral is

$$F_i = \int_{\partial A} d^2x \, \sigma_{ij} n_j \tag{1.22}$$

where n_j are the components of the unit vector oriented outwards. We can interpret σ_{ij} as the i-th compontent fo the force per unit area applied to a surface whose normal vector is along the j-th axis. It is important to note that the force F_i is exerted on the portion considered by the surrounding parts of the body. This means that the force exerted from the portion on its boundary is $\int_{\partial A} d^2x \, \sigma_{ij} n_j$, with n_j still oriented outwards, see Fig.1.2. For instance, if the only stresses are given by an internal pressure p, the stress tensor is $\sigma_{ij} = -p\delta_{ij}$.

1.1.5 Torque density

Often an additional condition is imposed to the stress tensor: it is required to be symmetric. The requirement follows from this argument. The moment of the

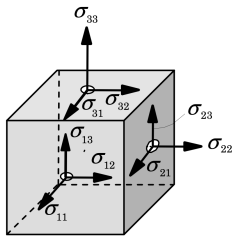

Figure 1.2: Stress tensor components. The first index refers to the face of the cube, the second refers to the direction of the force applied. The forces are applied on the cube by the surroundings.

force's density is

$$\mathbf{m} = \mathbf{f} \times \mathbf{x} = \star(\mathbf{f} \wedge \mathbf{x}) \tag{1.23}$$

where $\star$ denotes the Hodge star operator. The total moment of the force is $\mathbf{M} = \int_A \mathbf{m}$. Then

$$\begin{aligned}(\star M)_{ij} &= \int_A (\mathbf{f} \wedge \mathbf{x})_{ij} \\ &= \int_A d^3x\, f_i x_j - f_j x_i \\ &= \int_A d^3x\, (\partial_l \sigma_{il}) x_j - (\partial_l \sigma_{jl}) x_i \\ &= \int_A d^3x \partial_l (\sigma_{il} x_j) - \partial_l (\sigma_{jl} x_i) - (\sigma_{il}\partial_l x_j - \sigma_{jl}\partial_l x_i)\end{aligned} \tag{1.24}$$

Recognising the first two terms as boundary terms, we get

$$(\star M)_{ij} = \int_{\partial A} d^2x\, (\sigma_{il} x_j - \sigma_{jl} x_i) n_l - \int_A d^3x\, (\sigma_{ij} - \sigma_{ji}). \tag{1.25}$$

If $(\star M)_{ij}$ has to be a surface integral, then the last term must be zero and the stress must be symmetric. An antisymmetric stress is said to carry an *internal torque density*.

1.1.6 Equations of motion

If an external body force density $\mathbf{g}$ is applied to the elastic medium and the system is at equilibrium, the sum of the forces on each volume element must be zero. This means that

$$g_i + \partial_j \sigma_{ij} = 0. \tag{1.26}$$

The equations for the time-dependent dynamics are obtained by imposing that locally, the variation of the linear momentum is equally to the force. The linear momentum density is $\rho\dot{\boldsymbol{\xi}}$. Assuming a uniform density ρ we obtain

$$\rho\ddot{\xi}_i = \partial_j \sigma_{ij} + g_i \tag{1.27}$$

If the stress is expressed as a function of the displacement field with a *constitutive relation*, then Eq. 1.27 becomes a set of partial differential equations for the displacement field. Linear elasticity assumes a linear relation between the strain and the stress

$$\sigma_{ij} = C_{ijkl} u_{kl}. \tag{1.28}$$

The tensor C is called *elastic tensor*. The equations become $\rho\ddot{\xi}_i = C_{ijkl}\partial_j u_{kl} + g_i$. The strain is symmetric, thus without loss of generality the elastic tensor can be assumed to be symmetric in the last two indices. This allows to write finally

$$\rho\ddot{\xi}_i = C_{ijkl}\partial_j\partial_k\xi_l + g_i. \tag{1.29}$$

1.2 Symmetries and elastic tensor's structure

The symmetries of the system are reflected by the structure of the elastic tensor. We have already talked about the symmetry of the stress and of the strain. We now want to make a unified treatment in which all the symmetries are referred to the elastic tensor. We write the constitutive relations in a slightly more general way, employing the gradient of displacement instead of the strain, as in [25].

$$\sigma_{ij} = C_{ijkl}\partial_k\xi_l. \tag{1.30}$$

We remember that the strain is the symmetrized gradient of displacements.

In what follows, we assume that the material is homogeneous, which implies that C_{ijkl} does not depend on the position. The components of C_{ijkl} are known as *elastic moduli*, and they are the coefficients of proportionality between stress and strain that characterize the elastic behaviour of a solid.

The elastic tensor is a linear map between the gradient of displacement and the stress. These two are both rank-two tensors, thus the elastic tensor maps rank two tensors to rank-two tensors. The space of rank-two tensors is a vector space and obviously any basis can be chosen. It it partitularly useful to choose a basis that separates the irreducible representations of rotations. This is because many symmetry requirements involve rotations. We'll refer to these bases as the *geometrical bases*. We make explicit choices for 2D and 3D elasticity.

2D geometrical basis In 2D the basis we employ is:

$$\begin{aligned} \tau^D &= \begin{pmatrix} 1 & 0 \\ 0 & 1 \end{pmatrix} \qquad \tau^L = \begin{pmatrix} 0 & -1 \\ 1 & 0 \end{pmatrix} \\ \tau^{S_1} &= \begin{pmatrix} 1 & 0 \\ 0 & -1 \end{pmatrix} \quad \tau^{S_2} = \begin{pmatrix} 0 & 1 \\ 1 & 0 \end{pmatrix}, \end{aligned} \tag{1.31}$$

where τ^D is the identity matrix and, as always, lays in a trivial representation. τ^L is antisymmetric and lays in a trivial representation too, because it is the generator of SO(2) and thus commutes with every SO(2) matrix. τ^{S_1}, τ^{S_2} are symmetric traceless matrices and belong to a representation of SO(2) with charge two.

Both strain and stress can be decomposed onto this basis. The matrices are orthogonal but not nomalized with respect to the trace scalar product. Their product relations are $\tau_{ij}^{\alpha}\tau_{ij}^{\beta} = 2\delta_{\alpha\beta}$. Hence, the basis decomposition

$$(\nabla\xi)_{ij} = (\nabla\xi)_{\alpha}\tau_{ij}^{\alpha}, \tag{1.32}$$

(with $\alpha = D, L, S_1, S_2$) is obtained by defining

$$(\nabla\xi)_{\alpha} = \frac{1}{2}(\nabla\xi)_{ij}\tau_{ij}^{a} \tag{1.33}$$

Similarly, we have

$$\sigma_{ij} = \sigma_{\alpha}\tau_{ij}^{\alpha} \quad \text{, with} \quad \sigma_{\alpha} = \frac{1}{2}\sigma_{ij}\tau_{ij}^{\alpha}. \tag{1.34}$$

We can give a geometric interpretation of $(\nabla\xi)_{\alpha}$ and σ_{α}. $(\nabla\xi)_D$ represents a dilation, a change in area without change in shape or orientation. $(\nabla\xi)_L$ is an antisymmetric gradient of displacement that represents a rotation. $(\nabla\xi)_{S_1}, (\nabla\xi)_{S_2}$ are shears that change shape without changing area or orientation. $(\nabla\xi)_{S_1}$ measures shear strain with extension along the x axis and contraction along the y axis (or vice versa), $(\nabla\xi)_{S_2}$ has the axis of extension rotated 45° counterclockwise with respect to S_1. The interpretation of the stress components is analogous. σ_D is an isotropic stress, thus the negative of a pressure. σ_L is the antisymmetric component of the stress and thus a torque density. $\sigma_{S_1}, \sigma_{S_2}$ are stress shears.

In this basis, the elastic tensor becomes a matrix $C^{\alpha\beta}$, where a refers to the stress and b to the strain. The relations with C_{ijkl} is

$$C_{\alpha\beta} = \frac{1}{2}\tau_{ij}^{\alpha}C_{ijkl}\tau_{kl}^{\beta}, \tag{1.35}$$

and the constitutive relations are written as

$$\sigma_{\alpha} = C_{\alpha\beta}(\nabla\xi)_{\beta}. \tag{1.36}$$

We can give a graphical representation of Eq. 1.36.

$$\begin{pmatrix} \\ \\ \\ \\ \end{pmatrix} = 2 \begin{pmatrix} B & T & D_1 & D_2 \\ A & F & G_1 & G_2 \\ H_1 & I_1 & J_{11} & J_{12} \\ H_2 & I_2 & J_{21} & J_{22} \end{pmatrix} \begin{pmatrix} \\ \\ \\ \\ \end{pmatrix} \tag{1.37}$$

Here B is the bulk modulus that couples dilations to isotropic pressure, A is a modulus that associates internal torques to dilations, H_1, H_2 associate shear stresses to dilations. T, F, I_1, I_2 represent the four different kind of stresses that may be generated by a rotation of the medium. D_1, D_2 are the contributions to the pressure due to shear strains, G_1, G_2 are the contributions to the internal torque due to shear strains, $J_{\alpha\beta}$ are the shear stresses induced by shear strains.

3D geometrical basis In 3D we use the basis:

$$\begin{aligned}
\tau^{D}_{ij} &= \sqrt{\frac{2}{3}}\delta_{ij} & \tau^{L_k}_{ij} &= \epsilon_{ijk} \\
\tau^{S^1}_{ij} &= \frac{1}{\sqrt{3}}\begin{pmatrix} -1 & 0 & 0 \\ 0 & -1 & 0 \\ 0 & 0 & 2 \end{pmatrix} & \tau^{S^2}_{ij} &= \begin{pmatrix} 0 & 1 & 0 \\ 1 & 0 & 0 \\ 0 & 0 & 0 \end{pmatrix} \\
\tau^{S^3}_{ij} &= \begin{pmatrix} 1 & 0 & 0 \\ 0 & -1 & 0 \\ 0 & 0 & 0 \end{pmatrix} & \tau^{S^4}_{ij} &= \begin{pmatrix} 0 & 0 & 1 \\ 0 & 0 & 0 \\ 1 & 0 & 0 \end{pmatrix} \\
\tau^{S^5}_{ij} &= \begin{pmatrix} 0 & 0 & 0 \\ 0 & 0 & 1 \\ 0 & 1 & 0 \end{pmatrix}.
\end{aligned} \tag{1.38}$$

Here the basis elements are divided according to the irreducible representations of SO(3): matrices proportional to the identity, antisymmetric matrices and symmetric matrices. The identity matrix is a trivial representation (spin 0), the the antisymmetric matrices are the generator of SO(3) and lay in the adjoint representation, of spin 1. Finally there are five shear matrices, symmetric and traceless; these belong to a spin 2 representation. Like in the 2D case, the trace scalar product between the matrices is $\tau^{\alpha}_{ij}\tau^{\beta}_{ij} = 2\delta_{\alpha\beta}$, thus the same relations for the projection onto the geometrical basis hold and we can write

$$\begin{pmatrix} \sigma_D \\ \sigma_{R_1} \\ \sigma_{R_2} \\ \sigma_{R_3} \\ \sigma_{S_1} \\ \sigma_{S_2} \\ \sigma_{S_3} \\ \sigma_{S_4} \\ \sigma_{S_5} \end{pmatrix} = 2 \begin{pmatrix} \frac{3}{2}B & T_1 & T_2 & T_3 & D_1 & D_2 & D_3 & D_4 & D_5 \\ A_1 & F_{11} & F_{12} & F_{13} & G_{11} & G_{12} & G_{13} & G_{14} & G_{15} \\ A_2 & F_{21} & F_{22} & F_{23} & G_{21} & G_{22} & G_{23} & G_{24} & G_{25} \\ A_3 & F_{31} & F_{32} & F_{33} & G_{31} & G_{32} & G_{33} & G_{34} & G_{35} \\ H_1 & I_{11} & I_{12} & I_{13} & J_{11} & J_{12} & J_{13} & J_{14} & J_{15} \\ H_2 & I_{21} & I_{22} & I_{23} & J_{21} & J_{22} & J_{23} & J_{24} & J_{25} \\ H_3 & I_{31} & I_{32} & I_{33} & J_{31} & J_{32} & J_{33} & J_{34} & J_{35} \\ H_4 & I_{41} & I_{42} & I_{43} & J_{41} & J_{42} & J_{43} & J_{44} & J_{45} \\ H_5 & I_{51} & I_{52} & I_{53} & J_{51} & J_{52} & J_{53} & J_{54} & J_{55} \end{pmatrix} \begin{pmatrix} u_D \\ u_{R_1} \\ u_{R_2} \\ u_{R_3} \\ u_{S_1} \\ u_{S_2} \\ u_{S_3} \\ u_{S_4} \\ u_{S_5} \end{pmatrix}. \tag{1.39}$$

Or more concisely

$$\begin{pmatrix} \sigma_D \\ \sigma_{R_i} \\ \sigma_{S_\alpha} \end{pmatrix} = 2 \begin{pmatrix} \frac{3}{2}B & T_j & D_\beta \\ A_i & F_{ij} & G_{i\beta} \\ H_\alpha & I_{\alpha j} & J_{\alpha\beta} \end{pmatrix} \begin{pmatrix} u_D \\ u_{R_j} \\ u_{S_\beta} \end{pmatrix} \tag{1.40}$$

with in this case $i, j = 1, 2, 3$ and $\alpha, \beta = 1, 2, 3, 4, 5$. The most general elastic tensor has 16 independent elastic moduli in 2D and 81 in 3D.

We can now discuss how the symmetries affect the elastic tensor structure, both for C_{ijkl} and for $C_{\alpha\beta}$.

Rotation independence As we said before, the antisymmetric part of $\partial_i \xi_j$ represents rotations. A system in which any rotation does not induce a state of stress will have an elastic tensor with symmetry on the last two indices, thus $C_{ijkl} = C_{ijlk}$. In the geometrical basis, rotations are described by u_L in 2D and by u_{L_i} in 3D. If rotations do not induce any stress, then $C_{\alpha L} = 0$ and $C_{\alpha L_i} = 0$, so

$$\begin{pmatrix} \\ \\ \\ \\ \end{pmatrix} = 2 \begin{pmatrix} B & 0 & D_1 & D_2 \\ A & 0 & G_1 & G_2 \\ H_1 & 0 & J_{11} & J_{12} \\ H_2 & 0 & J_{21} & J_{22} \end{pmatrix} \begin{pmatrix} \\ \\ \\ \\ \end{pmatrix} \tag{1.41}$$

leaving 12 independent coefficients. In 3D we have

$$\begin{pmatrix} \sigma_D \\ \sigma_{R_i} \\ \sigma_{S_\alpha} \end{pmatrix} = 2 \begin{pmatrix} \frac{3}{2}B & 0 & D_\beta \\ A_i & 0 & G_{i\beta} \\ H_\alpha & 0 & J_{\alpha\beta} \end{pmatrix} \begin{pmatrix} u_D \\ u_{R_j} \\ u_{S_\beta} \end{pmatrix} \tag{1.42}$$

so $81 - 15 = 66$ independent moduli.

Internal torque A similar argument applies to the absence of torque density, which is described by the antisymmetric part of the stress. If the system has no internal torques, the stress tensor must be symmetric, and this must hold whatever deformation occurs. Necessarily, the elastic tensor is symmetric in the first two indices, which refer to the stress: $C_{ijkl} = C_{jikl}$. In the geometric basis the antisymmetric stresses are represented by τ^L and τ_i^L, thus we require $C^{R\alpha} = C^{R_i\alpha} = 0$ for every α i.e. no deformation can induce a torque density. In this case:

$$\begin{pmatrix} \\ \\ \\ \\ \end{pmatrix} = 2 \begin{pmatrix} B & T & D_1 & D_2 \\ 0 & 0 & 0 & 0 \\ H_1 & I_1 & J_{11} & J_{12} \\ H_2 & I_2 & J_{21} & J_{22} \end{pmatrix} \begin{pmatrix} \\ \\ \\ \\ \end{pmatrix} \tag{1.43}$$

and

$$\begin{pmatrix} \sigma_D \\ \sigma_{R_i} \\ \sigma_{S_\alpha} \end{pmatrix} = 2 \begin{pmatrix} \frac{3}{2}B & T_j & D_\beta \\ 0 & 0 & 0 \\ H_\alpha & I_{\alpha j} & J_{\alpha\beta} \end{pmatrix} \begin{pmatrix} u_D \\ u_{R_j} \\ u_{S_\beta} \end{pmatrix}. \tag{1.44}$$

Under this requirement there are still 12 free coefficients in 2D and 66 in 3D.

Isotropy The aforementioned symmetries were indeed internal symmetries of the strain and of the stress, we now consider symmetries that involve both at the same time. *Isotropy* is the requirement that the elastic properties are equal in any direction and thus that the elastic tensor is invariant under rotations. If the vectors transform with R_{ij}, isotropy requires that $C_{ijkl} = R_{ip}R_{jq}R_{ks}R_{lt}C_{pqst}$. Let's see what is the structure of an isotropic $C_{\alpha\beta}$. The basis elements transform with

$$\tau'^{\alpha}_{ij} = R_{im}\tau^{\alpha}_{mn}R^{\top}_{nj} =: \mathcal{R}_{\alpha\beta}\tau^{\beta}_{ij}, \tag{1.45}$$

for some $\mathcal{R}_{\alpha\beta}$ that represents rotations in the geometrical basis. Then the elastic tensor transforms according to $C'_{\alpha\beta} = \mathcal{R}_{\alpha\rho}\mathcal{R}_{\rho\sigma}C_{\sigma\beta}$. The elastic tensor is isotropic if

$$C_{\alpha\beta} = \mathcal{R}_{\alpha\rho}C_{\rho\sigma}\mathcal{R}^{\top}_{\sigma\beta} \tag{1.46}$$

For SO(2) it is easy to show that, given

$$R_{ij} = \begin{pmatrix} \cos\theta & \sin\theta \\ -\sin\theta & \cos\theta \end{pmatrix} \tag{1.47}$$

calculating explicitely $\mathcal{R}_{\alpha\beta}$ from Eq. 1.45 we get

$$\mathcal{R}_{\alpha\beta} = \begin{pmatrix} 1 & 0 & 0 & 0 \\ 0 & 1 & 0 & 0 \\ 0 & 0 & \cos(2\theta) & \sin(2\theta) \\ 0 & 0 & -\sin(2\theta) & \cos(2\theta) \end{pmatrix}. \tag{1.48}$$

Imposing that the 4×4 matrix $C_{\alpha\beta}$ commutes with $\mathcal{R}_{\alpha\beta}$ for every θ, we finally get the structure of the most general isotropic elastic tensor

$$\begin{pmatrix} \\ \\ \\ \\ \end{pmatrix} = 2 \begin{pmatrix} B & T & 0 & 0 \\ A & F & 0 & 0 \\ 0 & 0 & \mu & K^o \\ 0 & 0 & -K^o & \mu \end{pmatrix} \begin{pmatrix} \\ \\ \\ \\ \end{pmatrix} \tag{1.49}$$

In 3D we can use Schur's lemma, which states: *Let $\mathcal{D}$ be a complex irreducible representation of a group G on a finite-dimensional vector space V. If $T : V \to V$ is a linear operator such that*

$$T \circ \mathcal{D} = \mathcal{D} \circ T \quad \forall g \in G \tag{1.50}$$

then there exists $\lambda \in \mathbb{C}$ such that $T = \lambda \mathbb{I}_V$. For our usage, the role of $\mathcal{D}$ would be played by $\mathcal{R}$ (representation of rotations) and the role of T would be played by the elastic tensor.

We note that Schur's lemma can be applied to representations of SO(3) because the irreducible representations on the real field are irreducible also on the complex field. On the contrary, any SO(2) irreducible representation is reducible on the complex field into the direct sum of one-dimensional representation of U(1).

A 3D isotropic C has to be block diagonal on the irreducible representations. Furthermore, from Schur's lemma, the blocks must be proportional to the identity. Thus the elastic tensor reads

$$C_{\alpha\beta} = 2 \begin{pmatrix} \frac{3}{2}B & 0 & 0 \\ 0 & F\,\mathbb{I} & 0 \\ 0 & 0 & \mu\,\mathbb{I} \end{pmatrix} \tag{1.51}$$

Conservation of energy We will show in section 1.4 that if the internal forces are conservative (and thus, an elastic potential energy exists), the elastic tensor is symmetric under the exchange of the first two indices with the last two indices: $C_{ijkl} = C_{klij}$. In the geometrical basis the requirement is that the matrix $C_{\alpha\beta}$ must be symmetric, thus $T_i = A_i, D_\alpha = H_\alpha, G_{i\alpha} = H_{\alpha i}$ and $J_{\alpha\beta} = J_{\beta\alpha}$. In 2D under this requirement alone there remain 10 independent elastic moduli, while in 3D there remain 36.

Since energy is a fundamentally conserved quantity, a system that violates its conservation can not be isolated: it must be coupled to internal or external sources of energy. Integrating out the sources, the resulting system can display non-conservative phenomena.

Chirality A tensor is *achiral* if any parity operation (inversion of an odd number of spatial coordinates) is equivalent to a rotation, otherwise it is *chiral*. In 3D, the spatial inversion I_n of an axis $\hat{n}$ is equal to $-R_n(\pi)$ (a rotation of π around the axis), while an inversion of all the three axes is equal to $-\,\mathrm{id}$. Any tensor with an even rank (like the elastic tensor, which has four indices) is then achiral because the inversion of one axis acts like a rotation of π and the inversion of all the axes acts like the identity.

In 2D we can explicitly calculate the conditions for the elastic tensor to be achiral. Without loss of generality we consider reflections along the x-axis, which are implemented by the matrix

$$\tau^{S_1} = \begin{pmatrix} 1 & 0 \\ 0 & -1 \end{pmatrix}. \tag{1.52}$$

The elements of the geometrical basis transform as $\tau_{ij}^{\alpha} \mapsto \mathcal{I}_{\alpha\beta}\tau_{ij}^{\beta}$, with

$$\mathcal{I}_{\alpha\beta} = \begin{pmatrix} 1 & 0 & 0 & 0 \\ 0 & -1 & 0 & 0 \\ 0 & 0 & 1 & 0 \\ 0 & 0 & 0 & -1 \end{pmatrix}. \tag{1.53}$$

The strain and stress components transform with $\mathcal{I}_{\alpha\beta}$, too, and the elastic tensor transforms with $C_{\alpha\beta} \mapsto \mathcal{I}_{\alpha\rho}C_{\rho\sigma}\mathcal{I}_{\sigma\beta}$. Achirality requires that there exists a rotation such that its action is equivalent to that of the inversion. This is

$$\mathcal{I}_{\alpha\rho}C_{\rho\sigma}\mathcal{I}_{\sigma\beta} = \mathcal{R}_{\alpha\rho}C_{\rho\sigma}\mathcal{R}^{\top}_{\sigma\beta}. \tag{1.54}$$

with $\mathcal{R}_{\alpha\beta}$ given by Eq. 1.48. Applying the inversion we get

$$\begin{pmatrix} B & -T & D_1 & -D_2 \\ -A & F & -G_1 & G_2 \\ H_1 & -I_1 & J_{11} & -J_{12} \\ -H_2 & I_2 & -J_{21} & J_{22} \end{pmatrix}, \tag{1.55}$$

Under a rotation, the upper left 2×2 block remains unchanged, the elements D_i, G_i, H_i, I_i transform as vectors, $J_{ij} = R_{im}J_{mn}R^{\top}_{nj}$ (with R_{ij} a 2×2 rotation

matrix). We give an additional parametrization of the J_{ij} submatrix

$$J_{ij} = \begin{pmatrix} \mu + \gamma & \beta + K^o \\ \beta - K^o & \mu - \gamma \end{pmatrix}. \tag{1.56}$$

The elastic tensor is then achiral if

$$A = 0 \tag{1.57a}$$
$$T = 0 \tag{1.57b}$$
$$\vec{D} \parallel \vec{H} \tag{1.57c}$$
$$\vec{G} \parallel \vec{I} \tag{1.57d}$$
$$\vec{D} \perp \vec{G} \tag{1.57e}$$
$$K^o = 0 \tag{1.57f}$$
$$\beta(H_1^2 - H_2^2) - 2\gamma H_1 H_2 = 0. \tag{1.57g}$$

Here A and T are manifestly chiral coefficients because they couple rotations and dilations, so, if they are non-zero, an orientation is necessarily chosen. The others equations require that the vector of the shears that induce a pressure must be parallel to the shear stresses induced by dilation, that the shears that induce internal torque must be parallel to the shear stresses induced by rotations and that these two directions must be orthogonal. Lastly, Eq. 1.57g states that the axes that diagonalizes the symmetric shear coupling must either be parallel or perpendicular to the axis that couples shear and dilation.

1.3 Odd elasticity and other symmetries

A linear elastic system is odd elastic if it violates energy conservation. This is equivalent to saying that the elastic tensor has a non-vanishing antisymmetric (odd) part: $C^o_{ijkl} = -C^o_{klij}$. We call *odd moduli* or *active moduli* the non-symmetric components of the elastic tensor.

We accept the common assumption of rotation independence and thus consider systems in which only the variations of internal distances (the metric) produce stresses, and the constitutive relations can be written using the strain tensor instead of the gradient of the displacement.

1.3.1 Odd elasticity and isotropy

If we further assume isotropy, we need to distinguish 2D systems from the 3D ones.

2D In 2D we see that isotropy is compatible with odd elasticity and the most general elastic tensor with rotation independence and isotropy is the following

$$C_{\alpha\beta} = 2\begin{pmatrix} B & 0 & 0 & 0 \\ A & 0 & 0 & 0 \\ 0 & 0 & \mu & K^o \\ 0 & 0 & -K^o & \mu \end{pmatrix}. \tag{1.58}$$

Here have two odd elastic moduli: A and K^o. A represents the internal torques generated by dilations, while K^o is a coupling between shear strains and shear stresses. We can see the difference between K^o and μ, which deals with the shears, too. μ couples the shear strains to the shear stresses acting as the identity matrix on the shear space. Differently, K^o couples two different kinds of strains and does it in an antisymmetric way.

The passive moduli A and K^o are independent, odd elastic systems with $A = 0$ and $K^o \neq 0$ can exist.

3D In 3D, odd elasticity is not compatible with isotropy anymore. In fact, from equation 1.51, we see that a 3D isotropic elastic tensor must be diagonal in the geometrical basis, and thus it cannot have an antisymmetric part. We can reduce the requirements and study the compatibility of odd elasticity with cylindrical SO(2) isotropy.

3D with cylindrical symmetry Cylindrical isotropy is imposed requiring the elastic tensor to be invariant under any rotation along the z-axis. In order to do so, it must commute with the generator of rotations along the z axis, that, expressed in the geometrical basis, will be a 9×9 matrix $L_{\alpha\beta}$, the same size of $C_{\alpha\beta}$.

We now construct $L_{\alpha\beta}$. Let l_{ij} be the generator of rotations in the vector representation. Then $r_{ij} = \exp(\theta l)_{ij}$ is a rotation matrix. An element of the geometrical basis τ^α_{ij} transforms according to

$$\begin{aligned} \tau'^\alpha_{ij} &= (r\tau^\alpha r^\top)_{ij} \\ &= (e^{\theta l}\tau^\alpha e^{-\theta l})_{ij} = (\tau^\alpha + \theta\,[l, \tau^\alpha])_{ij} + O(\theta^2) \end{aligned} \tag{1.59}$$

But we can also write

$$\begin{aligned} \tau'^\alpha_{ij} &= R_{\alpha\beta}\tau^\beta_{ij} \\ &= (\delta_{\alpha\beta} + \theta L_{\alpha\beta} + O(\theta^2))\tau^\beta_{ij}. \end{aligned} \tag{1.60}$$

Equating the first order terms in θ we obtain

$$L_{\alpha\beta}\tau^\beta_{ij} = [l, \tau^\alpha]_{ij}\,. \tag{1.61}$$

Calculating explicitly the commutators in the previous equation we obtain:

$$L_{\alpha\beta} = \begin{pmatrix} 0 & 0 & 0 & 0 & 0 & 0 \\ 0 & 0 & 0 & 0 & 0 & 0 \\ 0 & 0 & 0 & 2 & 0 & 0 \\ 0 & 0 & -2 & 0 & 0 & 0 \\ 0 & 0 & 0 & 0 & 0 & 1 \\ 0 & 0 & 0 & 0 & -1 & 0 \end{pmatrix}. \tag{1.62}$$

Finally, taking a generic elastic tensor $C_{\alpha\beta}$ and imposing its commutator with $L_{\alpha\beta}$ to be zero, we get the structure of the most general isotropic elastic tensor. Imposing further rotation independence we get:

$$C = 2 \begin{pmatrix} \frac{3}{2}B & 0 & 0 & 0 & D+H & 0 & 0 & 0 & 0 \\ 0 & 0 & 0 & 0 & 0 & 0 & 0 & G_3 & G_2 \\ 0 & 0 & 0 & 0 & 0 & 0 & 0 & G_2 & -G_3 \\ A & 0 & 0 & 0 & G_1 & 0 & 0 & 0 & 0 \\ D-H & 0 & 0 & 0 & \mu_3 & 0 & 0 & 0 & 0 \\ 0 & 0 & 0 & 0 & 0 & \mu_1 & K_1^o & 0 & 0 \\ 0 & 0 & 0 & 0 & 0 & -K_1^0 & \mu_1 & 0 & 0 \\ 0 & 0 & 0 & 0 & 0 & 0 & 0 & \mu_2 & K_2^o \\ 0 & 0 & 0 & 0 & 0 & 0 & 0 & -K_2^o & \mu_2 \end{pmatrix}. \tag{1.63}$$

1.3.2 Odd elasticity and torque density

It is easy to see that odd elasticity is compatible with internal torque density. We can say more: if rotation independence is assumed, odd elasticity is necessary in order to have internal torques. In fact, under rotation independence we have $C_{ijkl} = C_{ijlk}$, if we add $C_{ijkl} = C_{klij}$, then $C_{ijkl} = C_{jikl}$ and the torque density is zero. Anyway, odd elasticity does not necessarily come with internal torques, even in the isotropic case. In 2D, if $A = 0$ and $K^0 \neq 0$, the system is odd elastic but with zero internal torques. Similarly, in 3D the moduli K_1^o, K_2^o are odd but not produce any internal torque.

1.3.3 Odd elasticity and chirality

As we said before, three dimensional odd elasticity is necessarily achiral. In 2D, the system is chiral if it violates any of the equations from Eq. 1.57a to Eq. 1.57e. If the system is additionally isotropic, and has rotation independence, then odd elasticity necessarily comes with chirality, as the moduli A and K^o are both odd and chiral.

If the system is anisotropic, then it may be achiral with odd elasticity, for instance with $\vec{D} = -\vec{H} =\neq 0$ and $A, T, \vec{G}, \vec{I} = 0$.

An anisotropic system may also be chiral without odd elasticity. For instance a solid with $D_1 = H_1$ and $\beta \neq 0$ with $D_2, H_2, \vec{G}, \vec{I}, \gamma, A, T, F, K^o = 0$. In this case, Eq. 1.57g is violated so the solid is chiral.

1.4 Work cycles

We now show that the elastic forces are conservative if and only if the elastic tensor has the major symmetry $C_{ijkl} = C_{klij}$.

Consider a volume element (it will be a surface element if the system is 2D) of the system and suppose that it undergoes a deformation $\boldsymbol{\xi}(t)$ in time – the spatial dependence is omitted because we are looking at a fixed position in space. The gradient of displacement then depends on time, too, so we write $(\partial_i \xi_j)(t)$. The forces are conservative and only if for every closed loop of deformation (i.e. for every deformation that starts at time t_i, ends at time t_f and such that $\boldsymbol{\xi}(t_\mathrm{i}) = \boldsymbol{\xi}(t_\mathrm{f})$) the work done is zero. The work per unit volume (area) done by the elastic forces developed inside the volume element on the surroundings when an infinitesimal deformation $d\boldsymbol{\xi}$ is performed is given by

$$đw = \sigma_{ij} d(\partial_i \xi_j). \tag{1.64}$$

The $đ$ symbol denotes that $đw$ may not be an exact differential. In fact, the infinitesimal work is a differential form over the space of gradient of displacements. The space is simply connected (is $\mathbb{R}^n$) so the form is exact if and only if it is closed, but the form may not be closed.

The work per unit volume under a finite cycle of deformation is calculated as a line integral. We consider a closed path Γ in the strain space, parametrized by $(\partial_i \xi_j)(t)$. By applying Stokes's theorem, we can express the work w as a surface integral, where the surface lays in the strain space, too.

$$\begin{aligned} w &= \oint_\Gamma \sigma_{ij} d(\partial_i \xi_j) \\ &= \int_\mathcal{S} \frac{1}{2} \frac{\partial \sigma_{ij}}{\partial(\partial_k \xi_l)} \, d(\partial_i \xi_j) \wedge d(\partial_k \xi_l) \\ &= \int_\mathcal{S} \frac{1}{2} C_{ijkl} d(\partial_i \xi_j) \wedge d(\partial_k \xi_l) \end{aligned} \tag{1.65}$$

With S a surface in strain space such that $\partial\mathcal{S} = \Gamma$. Since the wedge product is antisymmetric, the contributions to the integral are only given by the antisymmetric part of the elastic tensor

$$C^o_{ijkl} = 1/2(C_{ijkl} - C_{klij}). \tag{1.66}$$

The forces are conservative if and only if

$$C_{ijkl} = C_{klij}. \tag{1.67}$$

In the geometrical bases, energy conservation requires the elastic tensor to be a symmetric matrix, $C_{\alpha\beta} = C_{\beta\alpha}$.

In the presence of odd elasticity, the integral is in general non-vanishing. Let us consider an arbitrary basis in which the gradients of displacement are identified by the coordinates $(\nabla\xi)_a$, the stresses by σ_α and the elastic tensor,

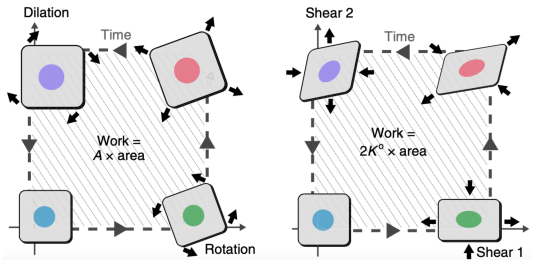

Figure 1.3: Two active cycles with a net amount of work injected or extracted from the system. **a,** An odd elastic material is subjected to a closed cycle in strain space. The system is first rotated by 45 degrees without doing work because there is no internal torque. Then applying a dilation, isotropic pressure and internal torque are generated. Due to the isotropic component, the environment does work on the system. Then the system is rotated and a finite work is done or extracted, depending on the sign of A. Finally, the system is allowed to contract to its original size, giving back the energy of the dilation to the environment. **b,** A cycle in the plane of shears. Due to antisymmetric coupling regulated by K^o, the works on opposite sides do not cancel each other, giving a non-zero total work.

being a linear operator, by $C_{\alpha\beta}$. We decompose the elastic tensor in the even and odd terms

$$C_{\alpha\beta} = C^e_{\alpha\beta} + C^o_{\alpha\beta}. \tag{1.68}$$

Where $C^e_{\alpha\beta} = C^e_{\beta\alpha}$ and $C^e_{\alpha\beta} = -C^e_{\beta\alpha}$. The work per unit volume can now be expressed as

$$w = \oint_\Gamma \sigma_\alpha d(\nabla\xi)_\alpha = \int_{\mathcal{S}} \frac{1}{2} C^o_{\alpha\beta} d(\nabla\xi)_\alpha \wedge d(\nabla\xi)_\beta. \tag{1.69}$$

If the path Γ lies in the plane spanned by two fixed basis elements $(\nabla\xi)_\rho, (\nabla\xi)_\sigma$, then the elastic tensor can be collected out of the integral and the work results to be equal to the odd modulus times the signed area in the strain space enclosed by the cycle: $C^o_{\rho\sigma}\,\mathrm{Area}\,\mathcal{S}$. These paths will be called *active cycles*.

Active cycles in two dimensions We can now study the active cycles in two dimensions. Consider an odd elastic isotropic system with elastic tensor given by Eq. 1.58. The antisymmetric part of the elastic tensor is

$$C^o_{\alpha\beta} = \begin{pmatrix} 0 & A & 0 & 0 \\ A & 0 & 0 & 0 \\ 0 & 0 & 0 & 2K^o \\ 0 & 0 & -2K^o & 0 \end{pmatrix}. \tag{1.70}$$

This tells us that performing a cycle that involves the first two components of the strain (dilations and rotations), the energy extracted is A times the area enclosed in the strain plane. Here is an example, depicted in Fig. 1.3a. One first

applies a dilation to the system an induces an internal torque proportional to the elastic modulus A. An isotropic pressure arises too, so that the environment does some work on the system. Then the system is rotated of some angle. The work of this transformation is proportional to A. Then, allowing the system to contract to its original size, the energy spent for the original dilation is sent back to the environment. The system has now no internal torque and can be rotated to its original position without spending energy. Overall, a finite amount of work proportional to A is injected into (or extracted from) the system.

1.5 Active waves

We consider the dynamics of an odd elastic system subjected to an external substrate drag force $-\Gamma\dot{\boldsymbol{\xi}}$. The equations of motion are

$$\rho\ddot{\xi}_i + \Gamma\dot{\xi}_i = C_{ijkl}\partial_j\partial_k\xi_l. \tag{1.71}$$

Activity can change drastically the dynamics. We now show that odd elasticity allows the propagation of waves even in the overdamped regime, the condition verified when inertia is irrelevant and the dynamics is governed by the balance the elastic forces with the drag. The overdamped equation are

$$\Gamma\dot{\xi}_j = C_{ijkl}\partial_i\partial_k\xi_l. \tag{1.72}$$

We consider a generic odd elastic isotropic system in which only the variation of internal distances induces a state of stress. The elastic tensor si

$$C_{\alpha\beta} = 2\begin{pmatrix} B & 0 & 0 & 0 \\ A & 0 & 0 & 0 \\ 0 & 0 & \mu & K^o \\ 0 & 0 & -K^o & \mu \end{pmatrix}, \tag{1.73}$$

and expressed in the four-indices form is

$$C_{ijmn} = B\delta_{ij}\delta_{mn} + \mu\left(\delta_{in}\delta_{jm} + \delta_{im}\delta_{jn} - \delta_{ij}\delta_{mn}\right) + K^o E_{ijmn} - A\epsilon_{ij}\delta_{mn}, \tag{1.74}$$

with

$$E_{ijmn} := \frac{1}{2}\left(\epsilon_{im}\delta_{jn} + \epsilon_{in}\delta_{jm} + \epsilon_{jm}\delta_{in} + \epsilon_{jn}\delta_{im}\right). \tag{1.75}$$

We study solutions in an infinite homogeneous system. The equations are linear, so we can look for plane waves of the form $\xi_i(\mathbf{x}, t) = \tilde{\xi}_i(\mathbf{q})e^{i\mathbf{q}\cdot\mathbf{x} - i\omega t}$. The equations in Fourier space become

$$-i\omega\Gamma\tilde{\xi}_j = -q_i q_m C_{ijmn}\tilde{\xi}_n \tag{1.76}$$

and, explicitly

$$\omega\Gamma\begin{pmatrix}\tilde{\xi}_x \\ \tilde{\xi}_y\end{pmatrix} = \begin{pmatrix} Bq_x^2 + \mu q^2 + Aq_x q_y & Bq_x q_y + K^o q^2 + Aq_y^2 \\ Bq_x q_y - K^o q^2 - Aq_x^2 & Bq_y^2 + \mu q^2 - Aq_x q_y \end{pmatrix}\begin{pmatrix}\tilde{\xi}_x \\ \tilde{\xi}_y\end{pmatrix}. \tag{1.77}$$

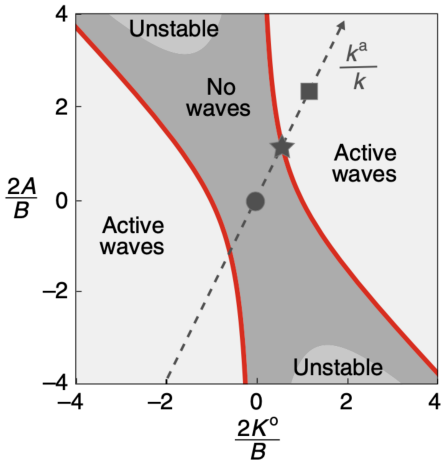

Figure 1.4: Phase diagram of the wave dynamics of an odd solid in the overdamped limit. In the dark grey region, the eigenmodes are exponentially damped in time. As the red line described by Eq 1.82 is crossed, active waves are able to propagate with a damping coefficient proportional to the passive moduli. Instabilities arise for $\tilde{A}$ greater than the threshold of Eq. 1.83.

A further simplification is obtained if we employ the polar basis in Fourier space. Let

$$\xi_\parallel = \hat{q}_i \tilde{\xi}_i \qquad \xi_\perp = \epsilon_{ij} \hat{q}_i \tilde{\xi}_i \tag{1.78}$$

with $\hat{q}_i = q_i/q$, $q = |\mathbf{q}|$ and ϵ_{ij} the two dimensional Levi-Civita symbol. Then the equations become

$$i\omega\Gamma \begin{pmatrix} \xi_\parallel \\ \xi_\perp \end{pmatrix} = q^2 \begin{pmatrix} B+\mu & K^o \\ -K^o - A & \mu \end{pmatrix} \begin{pmatrix} \xi_\parallel \\ \xi_\perp \end{pmatrix}. \tag{1.79}$$

The matrix on the right hand side, with the q^2 prefactor is called *dynamical matrix*. Diagonalizing the matrix the equations are decoupled, indeed the eigenvectors are called *eigenmodes*. The eigenvalues give us the dispersion relation of each eigenmode, i.e. the expression $\omega(\mathbf{q})$. We observe that due to isotropy the spectrum depends only on q^2, so the dispersion relation is $\omega(q)$. Calculating the eigenvalues we get

$$\omega = -i \left[\frac{B}{2} + \mu \pm \sqrt{\left(\frac{B}{2}\right)^2 - K^o A - (K^o)^2} \right] \frac{q^2}{\Gamma}. \tag{1.80}$$

Since the time dependence is $e^{-i\omega t}$, as long as the quantity in square brackets is real and positive, the eigenmodes are exponentially damped in time. On the contrary, a real ω implies wave propagation. If we define

$$\tilde{A} = \frac{A}{B/2} \quad \tilde{K}^o = \frac{K^o}{B/2} \quad \tilde{\mu} = \frac{\mu}{B/2}, \tag{1.81}$$

the threshold for wave propagation is given by

$$\tilde{A} = \frac{1}{\tilde{K}^o} - \tilde{K}^o \tag{1.82}$$

which is an hyperbola, represented by the red line in Fig. 1.4. If the frequency becomes real and negative, the modes are amplified in time. This is a sign of instability. The threshold for instabilities is given by

$$\tilde{A} = -\frac{\left(2\tilde{\mu} + \tilde{\mu}^2 + \left(\tilde{K}^o\right)^2\right)}{\tilde{K}^o}. \tag{1.83}$$

The instability regions are coloured in light gray in Fig. 1.4.

Chapter 2

Topological matter

In this chapter we introduce the main tools from topology that will be employed for the study of the normal modes of odd elastic plates. As we will see in chapter 4, the eigenspaces of the dynamical matrix, associated to the normal modes of the bulk, describe a vector bundle over the momentum space. The non-triviality of the bundle is reflected by the appearance of edge modes confined to the boundary of the system.

In section 1, we review the history of the use of topology in condensed matter physics, from the quantum Hall effect up to classical wave mechanics. In section 2 we introduce the mathematical notions of vector bundle and triviality of a bundle. In section 3 we specify the bundle structure of physical interest: the Bloch bundle, defined over the first Brillouin zone. In section 4 we present the Chern number, a topological invariant of the bundle that can be explicitly calculated and is related to the edge modes. In section 5 we give a broader description of the edge modes and express the principle of bulk-edge correspondence.

More mathematical details can be found in [26], a suggested introduction to topological insulators is [27].

2.1 From quantum to classical

The use of topology in condensed matter physics has its origins in the studies for the integer quantum Hall effect (IQHE).

In 1980 Von Klitzing [28] discovered that the Hall conductance of a two-dimensional electron gas subjected to a strong magnetic field shows plateaus for a range of the external magnetic field applied to the sample and that the phenomenon was insensitive to the shape of the device. In 1982 Halperin [29] showed that at the boundary of a system in the quantum Hall phase there exist quasi-one dimensional conducting states. These states propagate unidirectionally along the perimeter of the system—with direction (clockwise or anti-clockwise) according to the external magnetic field—and are robust when subjected to a moderate disordered potential. Another important result was obtained in

1982 too by Thouless, Kohomoto, Nightingale and den Nijs (TKNN) [30]. They studied the IQHE in the bulk and managed to relate the Hall conductance σ_H to the so called "TKNN integer", which was soon recognised to be the first Chern number of the bundle constituted by the Bloch eigenstates of the occupied bands [31].

In 1988 Haldane [32] proposed a model for the realization of IQHE in 2d systems without a strong magnetic field. His model makes use of a spatially varying magnetic field that allows for the breaking of time reversal symmetry, still with a vanishing flux on each unit cell. There, Haldane showed that the breaking of time-reversal symmetry was the essential element for the quantum Hall phase. This was the first example of a topological, or Chern, insulator.

In 1993 Hatsugai [33] obtained a result that could be considered the first rigorous statement of the *bulk-edge correspondence*. He defined a topological invariant that characterises the edge problem and showed that it is equal to the TKNN invariant for the bulk system. Thus, the twisted topology of the bulk electron bands is related to the existence of the edge modes.

In the following decades several developments occurred, both theoretical and experimental, leading to the discovery of new classes of topological insulator in 2D and 3D and of topological superconductors. However, until recent years the role of topology had been confined to quantum systems. In the 2000s, unidirectionally optical waveguides in photonic crystals were proposed [34], transcribing the key features of the Haldane model for topological insulators to photonic systems. There, the normal modes of Maxwell equations played the role of Bloch's eigenstates and time reversal symmetry was broken exploiting the Faraday effect. A recent review is [16]. Topological edge modes were studied for phononic systems, too [35]. Even more recently, in the 2010s, the floppy modes shown by isostatic lattices [36] were understood in the framework of topological band theory. A seminal work is [37], for a wider overview see [18].

Topological modes have been predicted also in hydrodynamical models for equatorial waves [22] in which time reversal symmetry is broken by Coriolis force. Formal analogues of this model have been found in active fluids and plasma physics [21], with further formal developements on the mathematical side and on the bulk-edge correspondence for such systems [38, 39]. In this thesis, we will show that flexural waves of odd elastic plates are described by this model, too.

2.2 Bundles

A smooth bundle is a triple (E, π, M) where E and M are smooth differentiable manifolds, called respectively *total space* and *base space* and $\pi : E \to M$ is a continuous and surjective map. We will often denote the bundle as $E \xrightarrow{\pi} M$.

We call the preimage under π of a point $p \in M$, the *fibre* at that point and denote it with F_p. The fibres are manifolds, as well. If, moreover, all the fibres are diffeomorphic to a given manifold, called *typical fibre* F, then the bundle is said to be a *fibre bundle*. We can think of the bundle as composed by the base manifold with a fibre attached to each point. A map $\sigma : M \to E$ is called a

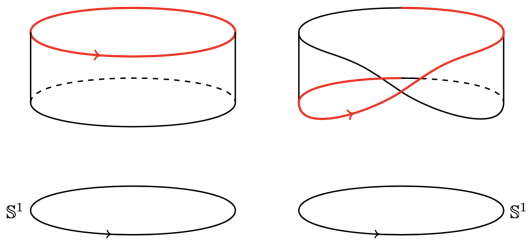

Figure 2.1: A cylinder (left) and a Möbius strip (right) are both fibre bundles with a circle $\mathbb{S}^1$ as base manifold and a segment $[-1, 1]$ as typical fiber. However, they are different manifolds.

(cross-)section of the bundle if $\pi \circ \sigma = \mathrm{id}_M$ i.e. associates to each point of the base manifold an element of the fibre at that point.

We now consider a common example of two similar but different bundles (Fig. 2.1. The Möbius strip is a two dimensional manifold that supports a bundle structure that has a circle $\mathbb{S}^1$ as base manifold and the segment $[-1, 1]$ as typical fibre. The cylinder is a two dimensional bundle with the same base manifold and the same typical fibre. However, it is a different manifold (the two are not diffeomorphic). What are the differences between the two bundles? Intuitively, the cylinder is "straight", while the Möbius strip is "twisted". The cylinder is an example of a *product bundle* because its topology is the same of the product of the base space with the fibre, while the Möbius strip is not. More generally:

Definition (Product bundle)**.** Let M and F be two manifolds. The triple $(M \times F, \pi_{\mathrm{t}}, F)$ with

$$\begin{aligned} \pi_{\mathrm{t}} : M \times F &\to M \\ (m, f) &\mapsto m \end{aligned}$$

is a *product bundle*. The map π_{t} is the *trivial projection map*.

Definition (Isomorphism of bundles)**.** Two bundles $E \xrightarrow{\pi} M$ and $E' \xrightarrow{\pi'} M'$ are isomorphic (as bundles) if there exist two diffeomorphism $f : M \to M'$ and $\phi : E \to E'$ such that the following diagram commutes

$$\begin{array}{ccc} E & \xrightarrow{\phi} & E' \\ \downarrow{\scriptstyle \pi} & & \downarrow{\scriptstyle \pi'} \\ M & \xrightarrow{f} & M' \end{array}$$

So that the fiber at $m \in M$ is mapped to the fiber at $u(m)$ and, furthermore, the total space E is mapped smoothly to the total space E'.

Definition (Trivial bundle)**.** A fibre bundle $E \xrightarrow{\pi} M$ with typical fibre F is *trivial* if it is isomorphic to a product bundle.

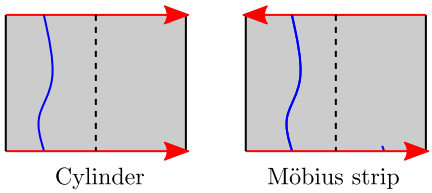

Figure 2.2: Gluing two opposite sides of a square one obtains a cylinder or a Möbius strip, depending on the orientation (red arrows). In the former case, a smooth non vanishing section (blue line) is allowed; in the latter, a non-vanishing global section is necessarily discontinuous.

We can now compare the two bundles considered in the previous example. The cylinder is trivial because it is a product bundle, while the Möbius strip is not trivial. Indeed, we could find the diffeomorphism f for the base manifolds (the identity, for instance) and we could also find an invertible map ϕ that acts fiberwise and "rotates" the fibers in order to match the cylinder, but there is no way this map can be a diffeomorphism between the total spaces. The fibers should be rotated in a discontinuous way.

We could still observe that, locally, a patch of a Möbius strip looks exactly the same as a patch of a cylinder. In fact, the Möbius strip is locally a product bundle and thus is said to be *locally trivial*. Let U be an open subset of M and $\phi : U \times F \to \pi^{-1}(U)$ a diffeomorphism such that $\pi \circ \phi(m, f) = p$. The map ϕ is called *local trivialization*. So we are requiring the following diagram to be commutative

$$\begin{array}{ccc} U \times F & \xrightarrow{\phi} & \pi^{-1}(U) \\ & {\scriptstyle \pi_t} \searrow \quad \swarrow {\scriptstyle \pi} & \\ & U & \end{array}$$

Non-triviality is a fundamental property relevant for physical applications. We are thus interested in tools that allow us to distinguish a trivial bundle from a non-trivial one. We now consider bundles with additional structures and give a first characterization of trivial bundles.

Definition. A *vector bundle* (E, π, M, F, G) is a fibre bundle $E \xrightarrow{\pi} M$ with typical fibre F endowed with a vector space structure and a left action of the group G on F.

Theorem. *A vector bundle with typical fiber of dimension n is trivial if and only if there are n smooth sections that form a basis on each fibre.*

If we consider the infinite Möbius strip with fiber $F = \mathbb{R}$, we can verify the statement of the theorem. In this case, the fibres are one dimensional, so the requirement is to have a non vanishing smooth section. It easy to see that this is not possible (Fig. 2.2), while it is possible for the cylinder.

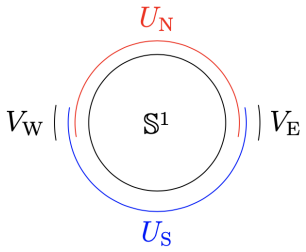

Figure 2.3: Schematic view of the open covering (U_N, U_S). The transition map is defined on the intersection $V_W \cup V_E$

Transition functions Another criterion for triviality deals with the *transition functions*. Consider two local trivializations ϕ_i and ϕ_j defined on U_i and U_j with $U_i \cap U_j \neq \emptyset$. We call *transition map* the function t_{ij} that at each $m \in U_i \cap U_j$ associates the element $g \in G$ that, applied to F, connects the two trivializations. More precisely

$$\begin{aligned} t_{ij} : U_i \cap U_j &\to G \\ m &\mapsto t_{ij}(m) = g \end{aligned}$$

such that

$$\phi_i(m, f) = \phi_i(m, gf).$$

If the bundle can be continuously deformed such that all the transition functions are the identity function, the bundle is trivial. Consider again the real-line vector bundle over $\mathbb{S}^1$. Let $U_N = (-\epsilon, \pi + \epsilon)$ and $U_S = (\pi - \epsilon, 0 + \epsilon)$ be an open covering $\mathbb{S}^1$ parametrized by $\theta \in [0, 2\pi)$. The two open set overlap at $V_W = (\pi - \epsilon, \pi + \epsilon)$ and $V_E = (-\epsilon, \epsilon)$, thus the transition funciton is defined on $U_N \cup U_S = V_W \cup V_E$ (Fig. 2.3). The structure group is $GL(1, \mathbb{R})$. The two local trivializations are isomorphic to two rectangular stripes. If we choose the transition function

$$t_{NS}(\theta \in V_W) = 1 \qquad t_{NS}(\theta \in V_E) = 1 \tag{2.1}$$

we are gluing the two stripes matching the borders with the same orientation, and we get a cylinder. If we choose the transition function

$$t_{NS}(\theta \in V_W) = 1 \qquad t_{NS}(\theta \in V_E) = -1 \tag{2.2}$$

the borders are matched differently, we add a twist and we get a Möbius strip.

2.3 Bloch bundles

The vector bundles which we will deal with are Bloch bundles, whose theory was initially developed for the quantum theory of electrons in periodic systems. We consider a single particle Hamiltonian with discrete translational symmetry.

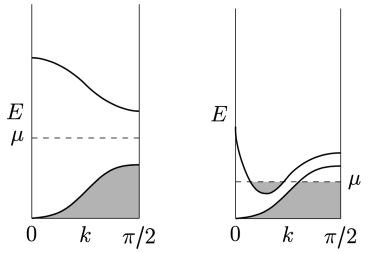

(a) Insulator. **(b)** Metal.

Figure 2.4: Examples of band structures over the first Brillouin zone. An insulator has a band gap and the Fermi energy lays in the gap. On the contrary, the bands of a metal have an energy overlap and the Fermi energy crosses both the valence and conducting bands.

The discrete translations form a lattice in the d-dimensional space, called the Bravais lattice, denoted with Γ. It is an abelian group isomorphic to $\mathbb{Z}^d$. As usual, the eigenstates of the Hamiltonian are classified by the unitary irreducible representations of the symmetry group. In this case, since the group is abelian, the irreducible representations are one dimensional and they can be expressed in the form of $e^{i\mathbf{k}\cdot\mathbf{r}}$ for $\mathbf{r} \in \Gamma$, labelled by the vector $\mathbf{k}$. The set of $\mathbf{k}$ vectors is usually called *first Brillouin zone* or simply *Brillouin zone* (BZ). Sometimes, we will call it *momentum space*. It has an abelian group structure, by addition of the $\mathbf{k}$ vectors. The topology of the BZ is that of a d-dimensional torus $\mathbb{T}^d$ because, for each $\mathbf{G}$ in the reciprocal space of Γ, $\mathbf{k}$ and $\mathbf{k} + \mathbf{G}$ label the same representation. The Brillouin zone, together with the topological structure and the group structure constitutes the Pontryagin dual of the Bravais lattice. The eigenstate labelled by $\mathbf{k}$ is thus

$$\psi_{\mathbf{k}}(\mathbf{x}) = e^{i\mathbf{k}\cdot\mathbf{x}} u_{\mathbf{k}}(\mathbf{x}), \quad u_{\mathbf{k}}(\mathbf{x}+\mathbf{r}) = u_{\mathbf{k}}(\mathbf{x}), \quad \mathbf{r} \in \Gamma, \quad \mathbf{k} \in BZ \tag{2.3}$$

which is the statement of Bloch's theorem.

The functions $u_{\mathbf{k}}(x)$ satisfy a Schrödinger equation with another Hamiltonian $\mathcal{H}(\mathbf{k})$, called Bloch Hamiltonian, parametrized by $\mathbf{k} \in BZ$. The eigenstates of $\mathcal{H}(\mathbf{k})$ at a given $\mathbf{k}$ are labelled by n, so that we can denote them by $|u_n(\mathbf{k})\rangle$. The eigenvalue equation for the Bloch's Hamiltonian is

$$\mathcal{H}(\mathbf{k}) \, |u_n(\mathbf{k})\rangle = E_n(\mathbf{k}) \, |u_n(\mathbf{k})\rangle \tag{2.4}$$

and the energies $\{E_n(\mathbf{k}) | \mathbf{k} \in \mathbb{T}^d\}$ at fixed n constitutes the n-th *band*.

We know from the axioms of quantum mechanics that the physical states are not uniquely represented of the Hilbert space: a multiplication with a (non-zero) complex number leaves the physical state unchanged. If we consider only normalized states, there remains the freedom of a phase multiplication. Geometrically, the states of the n-th band constitute a vector bundle over the

Brillouin zone, where the n-th eigenspace of $\mathcal{H}(\mathbf{k})$ is attached each $\mathbf{k} \in BZ$ and the phase freedom sets U(1) as the structure group. The eigenspaces are one-dimensional, so the states of a Bloch band constitute a complex line bundle over the Brillouin zone, which we call the *n-th band Bloch bundle*

$$\mathcal{L}_n \to BZ. \tag{2.5}$$

A choice of an eigenvector for each element of the momentum space constitutes a section of the Bloch bundle

$$\begin{aligned} |u_n\rangle : BZ &\to \mathcal{L}_n \\ \mathbf{k} &\mapsto |u_n(\mathbf{k})\rangle . \end{aligned} \tag{2.6}$$

We stress that this line bundle structure is well defined only for bands that do not cross any other band. When two bands cross, the bundle of each band cannot be defined because the eigenspace at the crossing $\mathbf{k}$ becomes two dimensional and there is not an unique way to choose which part belongs to one band and which part belongs to the other.

Topological insulators In an insulator, the filled bands and the unfilled bands are separated by an energy gap, where the Fermi energy sits (Fig. 2.4. Only excitations greater than the gap will produce a current in the sample. A topological insulator is an insulator with non-trivial filled bands. It is effectively an insulator in the bulk, but displays ungapped conducting states at the boundary.

A non-trivial bundle structure would be possible also for a metal, as long as the bands do not intersect one another. However, the edge states connecting different bands are more difficult to observe because the edge transport will be hidden by the bulk transport.

2.4 Chern number

We now ask ourselves how many different Bloch bundles can be constructed on a given momentum space? And how much do they differ from the trivial bundle? A complete answer would require a complete classification of complex line bundles, which is a difficult task we are not able to fulfil. However we can give a necessary condition for two Bloch bundles to be isomorphic: they have to be in the same first Chern class.

Chern classes are topological invariants for complex vector bundles. This means that if two bundles are equivalent, they lay in the same Chern class; the converse is not necessarily true. For $U(1)$ bundles, the only relevant Chern class is the first Chern class, which is the complex analogue of the Euler class and measures how much "twisted" the bundle is. For line bundles over 2d manifolds, the different first Chern classes are identified by an integer number, the first Chern number $\mathcal{C} \in \mathbb{Z}$. As one may guess, the trivial bundle has a vanishing Chern number. The number can be evaluated integrating the curvature F of

the vector bundle over the base manifold

$$\mathcal{C} = \frac{1}{2\pi} \int_{BZ} F. \tag{2.7}$$

The curvature F originates from a choice of a connection A on the vector bundle. Different connections can be chosen, which will induce different curvatures. In Eq. 2.7 we are using the powerful Chern-Gauss-Bonnet theorem, that allows to evaluate a property that is topological and does not depend on the connection (the Chern number) by using a quantity that depends on the connection (the curvature). This is strictly analogous to what happens for real vector bundles. There, the twisting of the bundle is identified by the Euler number. If we restrict our attention to the tangent bundle of two dimensional manifolds, the Euler number coincides with the Euler characteristic χ, which is a topological invariant of the manifold. Gauss-Bonnet theorem relates the Euler characteristic to the integral of the Gaussian curvature K of the manifold via

$$\chi = \frac{1}{2\pi} \int_{M} K da. \tag{2.8}$$

Here we remember that the Gaussian curvature depends on the metric of the manifold but the Euler characteristic does not. In this sense the Chern–Gauss–Bonnet theorem is a generalization of the Gauss–Bonnet theorem.

Let's return to the n-th band Bloch bundle. We now denote the states of a given band with $|u(\mathbf{k})\rangle$, omitting the band label. As we said, different connections may be chosen, and they all give rise to the same Chern number. A natural choice is the *Berry connection*, whose local form is given by

$$A(\mathbf{k}) = \frac{1}{i} \langle u(\mathbf{k})| \, d \, |u(\mathbf{k})\rangle \, . \tag{2.9}$$

In the mathematical vocabulary, the connection is the Lie-algebra valued one form defined on the vector bundle. Given a local section of the vector bundle, one can pull-back the connection, obtaining a Lie-algebra valued one form on the base manifold, called the *local form of the connection*. In physics, the expression *Berry connection* refers to the latter object. If the section $|u_n(\mathbf{k})\rangle$ is well defined and smooth for each $\mathbf{k} \in BZ$, then bundle is trivial. Conversely, the impossibility to have a global section of the bundle then implies that the Berry connection is not a single function defined globally.

Covering the Brillouin zone with open sets, a local section $|u(\mathbf{k})\rangle$ can be defined on each open set. On the intersection of two open sets, the two local sections are related by a $U(1)$ gauge map that has the same role of the transition map defined before. Let U_i and U_j be two open sets of BZ with non-zero intersection and let $\left|u^{(i)}(\mathbf{k})\right\rangle$ and $\left|u^{(j)}(\mathbf{k})\right\rangle$ be the two local sections. The gauge map function is a map

$$t : U_i \cap U_j \to U(1) \tag{2.10}$$

such that

$$\left|u^{(i)}(\mathbf{k})\right\rangle = t(\mathbf{k}) \left|u^{(j)}(\mathbf{k})\right\rangle \tag{2.11}$$

with

$$t(\mathbf{k}) = e^{i\phi(\mathbf{k})}. \tag{2.12}$$

Then from Eq. 2.9 the Berry connections obtained through the two sections are related by

$$A^{(i)} = A^{(j)} + d\phi. \tag{2.13}$$

The Berry curvature is defined on each open set as the exterior derivative of the Berry connection

$$F = dA. \tag{2.14}$$

Since $d^2\phi = 0$, F is gauge invariant. It depends on the connection but does not depend on the chosen section of the bundle (or gauge choice).

2.5 Edge modes

The topological structure of the bulk bands can show up in the physics at interfaces. If a topological insulator is put in contact with a trivial insulator or vacuum, chiral edge modes emerge at the interface between the two. An heuristic argument is the following.

The Brillouin zone, the Bloch bundle and the Chern number are mathematically defined for infinite systems, but their concrete use is for the bulk of finite systems. If we add an interface, we can not consider the system to be in the bulk, as it is obvious. However, in order to have a qualitative intuition, we could think at the interface as something that perturbs the bulk's properties. Imagine to parametrize the direction perpendicular to the interface with the coordinate y, such that the interface is at $y = 0$. At large negative values of y the system is in the bulk and has a defined value of the Chern number. At positive large values of y, the system is in the bulk too and has a different value of the Chern number. We could consider y as an external parameter, that continuously changes the bundle structure. The only way a continuous deformation can change the bundle structure is by closing the gap. So at the boundary we have the existence of ungapped (conducting) states, called *edge modes*. The edge modes propagate unidirectionally along the interface. Thus, for two dimensional systems, the have a one-dimensional wave vector k_x. The edge modes have frequencies in the gap and connect consecutive gapped bands.

Bulk-edge correspondence The link between topology and the edge modes is even more strong and goes under the name of *bulk-edge correspondence*. For topological insulators placed in contact with vacuum, the principle is expressed as follows [33]. Assume that the bands are labelled by the integer n. Let $N_{n,+}$ be the signed number of modes that leave $(+1)$ or join (-1) the n-th band from

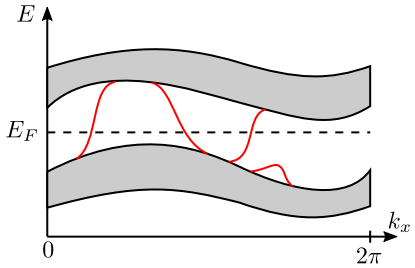

Figure 2.5: In grey, the bulk bands; for a given k_x, many energies can be covered, varying k_y. The red lines represent the (unidimensional) edge modes. In this case, the Chern number of the bottom band is $+1$, while the Chern number of the top band is -1.

above. Let $N_{n,-}$ be the signed number of modes that join $(+1)$ or leave (-1) the n-th band from below. The bulk-edge correspondence states that

$$\mathcal{C}_n = N_{n,+} - N_{n,-}, \tag{2.15}$$

where $\mathcal{C}_n$ is the Chern number of the n-th band.

For topological insulators, the relevant edge modes are those that connect the valence band to the conducting band (the conducting modes). These are the modes that cross the Fermi energy. In this case, the bulk-edge correspondence can be stated as follows. Let $N^\sharp$ be the number of modes that cross the Fermi energy and let v the integer label of the valence band. Then it is easy to see that

$$N^\sharp = N_{v,+} = N_{v+1,-}. \tag{2.16}$$

i.e. the number of modes that cross the Fermi energy is equal to the (net) number of modes that leave the valence band and equal to the (net) number of modes that join the conducting band. Then, rewriting the number of modes $N_{v,+}$ with respect to the Chern number and iterating we can rephrase the bulk-edge correspondence as

$$N^\sharp = \sum_{n \leq v} \mathcal{C}_n. \tag{2.17}$$

While rigorous proofs of bulk-edge correspondence for quantum topological insulators models have been obtained, the issue is still open for classical hydrodinamical models [38, 39], where the bulk-edge correspondence has to be taken in its weaker form. It remains a "guiding principle" that tells us that if the bulk is non-trivial, then there should be edge modes at the boundary of the system.

Chapter 3

Odd plates

The goal of this chapter is to derive the equations of motion of an odd elastic plate and identify its active cycles of deformations.

A plate is a three dimensional object that can be described as a two dimensional system because it is thin in one dimenson. More precisely, the three dimensional displacement field of a plate is reparametrized involving fields that are defined on the mid-plane of the plate, which is a two dimensional manifold. These fields satisfy a set of differential equations, that can be obtained from the three dimensional theory through the principle of virtual work.

In section 1 we set up the two-dimensional description of the plate, characterizing the displacement field, the strain and the stress tensor. In section 2 we introduce the principle of virtual work and derive the general structure of the equations that govern the plate's dynamics. In section 3 we derive the constitutive relations of a plate with cylindrical isotropy and no internal torques, applying a reduction procedure from the constitutive relations of the material in the three-dimensional bulk. In section 4 we use the constitutive relations to study the active cycles of deformations and in section 5 we explicitly obtain the equations of motion for the plate.

3.1 Plate description

3.1.1 The kinematical hypotheses

A plate is a structural object whose thickness is significantly smaller than the other two planform dimensions. It is a three dimensional system that can be deformed in all the three directions (Fig. 3.1). Thus, the displacement field $\boldsymbol{\xi}$ is a three dimensional vector field, defined over the whole plate.

We consider a flat plate of uniform thickness h whose midplane lies in the xy-plane. The plate theory is developed making a guess on the form of the displacement field and stress field, according to some kinematical and dynamical hypotheses. The displacement field is expanded in powers of z—the coordinate

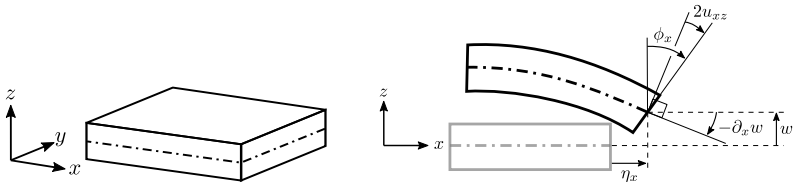

(a) Plate at rest. **(b)** Deformed plate.

Figure 3.1: A plate at rest and a deformed plate. η_x and w describe respectively the horizontal and vertical displacement of the mid plane. ϕ_x quantifies the deviation of the transverse normals towards the x-axis, while $-\partial_x w$ quantifies the bending of the midplane. The difference of the latter two is twice the transverse strain u_{xz}.

that runs through the thickness of the plate. Considering a displacement field that varies in time, we have

$$\xi_i(x, y, z, t) = \sum_{n=0}^{N} z^n \varphi_i^{(n)}(x, y, t). \tag{3.1}$$

The coefficients of the expansion $\varphi_i^{(n)}$ are the dynamical fields, defined on the two-dimensional horizontal mid-plane [40]. The precise expression for Eq.3.1 depends on the chosen kinematical hypotheses. In this work, we attend ourselves to the so-called Reissner-Mindlin theory. This requires that [40]

1. Straight lines perpendicular to the mid-surface (i.e., transverse normals) before deformation remain straight after deformation.
2. The transverse normals do not experience elongation (i.e., they are inextensible).

The inextensibility of the transverse normals implies that the normal strain u_{zz} is identically zero. Since $u_{zz} = \partial_z \xi_z$, then ξ_z does not depend on z and we get

$$\xi_z(x, y, z) = w(x, y). \tag{3.2}$$

Hence, the power expansion in z for the vertical displacement is truncated to the zero-th order.

The first hypothesis is then satisfied by requiring that the horizontal displacements have only a z-independent and a z-linear term, so that the transverse normals are reoriented but not bent. Labelling the horizontal components by $\alpha \in \{x, y\}$, we have

$$\xi_\alpha(x, y, z) = \eta_\alpha(x, y) + z\phi_\alpha(x, y). \tag{3.3}$$

We observe that η_α describes the horizontal displacement of the mid-plane ($z = 0$). The field ϕ_α describes a rotation of the transverse normals. ϕ_x quantifies the tilting towards the x-axis, while ϕ_y quantifies the tilting towards the y-axis (Fig. 3.1b).

3.1.2 Plate strain

The strain tensor can be calculated explicitly. We obtain

$$u_{\alpha\beta} = \partial_{(\alpha}\eta_{\beta)} + z\partial_{(\alpha}\phi_{\beta)} \tag{3.4a}$$

$$u_{\alpha z} = \frac{1}{2}(\phi_\alpha + \partial_\alpha w) \tag{3.4b}$$

$$u_{zz} = 0 \tag{3.4c}$$

Here $\alpha, \beta \in \{x, y\}$ and the round brackets indicate symmetrized indices. The horizontal strains $u_{\alpha\beta}$ have both a z-independent and a z-linear term, which we express as

$$u_{\alpha\beta} = u^0_{\alpha\beta} + z u^1_{\alpha\beta} \tag{3.5}$$

and thus we have

$$u^0_{\alpha\beta} = \partial_{(\alpha}\eta_{\beta)} \qquad u^1_{\alpha\beta} = \partial_{(\alpha}\phi_{\beta)}. \tag{3.6}$$

The term $u^0_{\alpha\beta}$ depends only on the fields η_α and describes horizontal strains that are uniform over the thickness of the thickness. The term $u^1_{\alpha\beta}$ describes horizontal strains in which the top face and the bottom face are deformed oppositely, as they have opposite values of the coordinate z. The midplane, originally laying horizontally, can be bent by the deformation. The tangent to the mid-plane that points in the α-direction is rotated vertically by an amount of $\partial_\alpha w$ (if w grows with x, then the tangent is rotated upwards). After the deformation, the transverse normal may not be orthogonal to the mid-plane anymore. In fact, the re-orientation of the transverse normal is quantified by ϕ_α, which is independent from w. The non-orthogonality between the deformed midplane and the deformed transverse normal is quantified by the transverse strain $u_{\alpha z}$, as shown in (3.4b) (see Fig. 3.1b).

We note that while the z-independent planar strains $u^0_{\alpha\beta}$ depend only on the horizontal displacements η_α and the z-linear planar strains $u^1_{\alpha\beta}$ depend only on the angular degrees of freedom, the transverse strains $u_{\alpha z}$ depend on two different kind of fields: the vertical displacement and the angular fields. This introduces a coupling between w and ϕ_α, the fields that describe the *bending deformations*. The *planar deformations* are described by the horizontal displacements η_α.

We choose a basis for the strains that separates the irreducible representations of rotations around the z-axis. This basis spans the space of symmetric matrices and will be called the *geometrical basis of the plate*.

$$\begin{aligned} D_{ij} &= \begin{pmatrix} 1 & 0 & 0 \\ 0 & 1 & 0 \\ 0 & 0 & 0 \end{pmatrix} & P_{ij} &= \begin{pmatrix} 0 & 0 & 0 \\ 0 & 0 & 0 \\ 0 & 0 & 1 \end{pmatrix} \\ S^1_{ij} &= \begin{pmatrix} 1 & 0 & 0 \\ 0 & -1 & 0 \\ 0 & 0 & 0 \end{pmatrix} & S^2_{ij} &= \begin{pmatrix} 0 & 1 & 0 \\ 1 & 0 & 0 \\ 0 & 0 & 0 \end{pmatrix} \\ T^x_{ij} &= \begin{pmatrix} 0 & 0 & 1 \\ 0 & 0 & 0 \\ 1 & 0 & 0 \end{pmatrix} & T^y_{ij} &= \begin{pmatrix} 0 & 0 & 0 \\ 0 & 0 & 1 \\ 0 & 1 & 0 \end{pmatrix} \end{aligned} \tag{3.7}$$

Here D and P are in the trivial representation. D represents planar dilations, while P represents vertical elongations. S^1, S^2 span planar shears in which an axis is dilated in one direction and the orthogonal in the plane is contracted. The two matrices are in representation of charge two; intuitively, the planar shear is identified by the axis of dilation, without information on it direction. S^1 dilates the x-axis, while S^2 dilates an axis that is 45° rotated from the x-axis. T^x and T^y represent transverse shears, in the plane xz and yz. These are in a representation of charge one, labelled by a direction in the xy-plane.

Projecting the strain onto the geometrical basis we obtain respectively $u_D, u_{S^1}, u_{S^2}, u_{T^x}, u_{T^y}$. We note that the basis elements D, S^1, S^2 involve the planar coordinates x, y, thus the relative strain components will have a z-independent term and a z-linear term. The strains relative to T^x and T^y will only have the z-independent term.

A visual representation is given in the following figure. Each image represents a deformation that produces a uniform non-zero value of the strain identified by the rows and columns and a zero value for all the other strains.

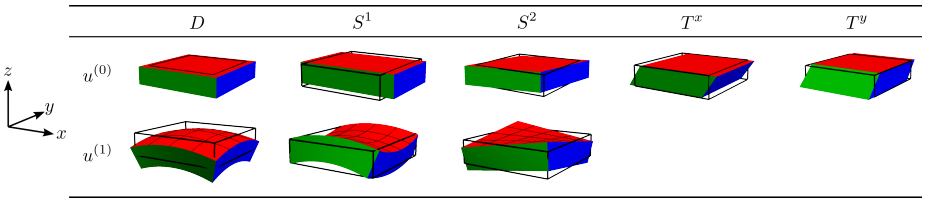

Figure 3.2: Different strains of a plate in the Reissner-Mindlin theory. Columns refer to the basis element, rows indicate whether the z-independent or the z-linear term is considered. We recall that $u_{zz} = 0$, thus $u_P = 0$ and that $u^1_{T^\alpha} = 0$ by construction, thus they are not represented.

3.1.3 Plate stress

We express the stress tensor in the geometrical basis of the plate and give an interpretation of the components.

σ_D represents a planar stress with cylindical symmetry, σ_P represents the normal stress σ_{zz}, σ_{S^1} and σ_{S^2} are planar shear stresses, while σ_{T^x} and σ_{T^y} are the transverse stresses.

As we already said, the plate is a three dimensional solid, described as a two dimensional system. The third dimension that runs along the thickness of the plate is literally "integrated out", as we show in section 3.2, where we derive the equations of motion. We will also see that the relevant dynamical quantities are the zero-th and the first moment in z of the stress. These are the **net stress**

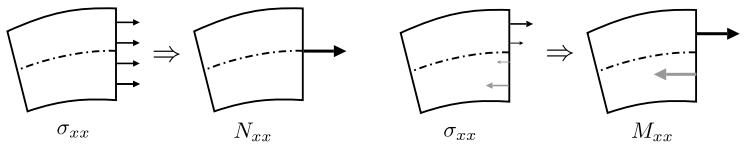

(a) Net stress. **(b)** Moment.

Figure 3.3: An example of net stress and moment relative to the stress component σ_{zz}. We show two stress distribution that produce a non-zero net stress and a non-zero moment.

tensor N_{ij} and the **moment tensor** M_{ij}, defined by

$$N_{ij} = \int_{-h/2}^{h/2} dz\, \sigma_{ij} \tag{3.8}$$

$$M_{ij} = \int_{-h/2}^{h/2} dz\, z\sigma_{ij}, \tag{3.9}$$

see Fig. 3.3 for a visual intuition.

We give a visual representation of the net stresses and the moments in the geometrical basis in the following image. The net stresses are represented by a single arrow on each face, while the moments are represented by a couple of opposite arrows on each face, as introduced in Fig. 3.3. We omit the components along the basis element P and the transverse moments M_{T^α}. because they are identically zero in our system, as we will show in section 3.3.

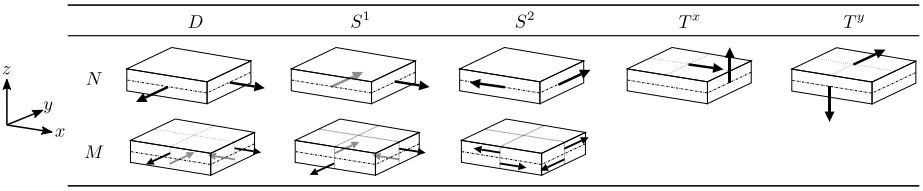

Figure 3.4: Irreducible components of the net stress and moment tensor. The grey arrows are pointing towards the inside of the plate

3.2 Virtual work

3.2.1 The principle of virtual work

The equations that govern the dynamics of a continuum system can be derived either with the Newton's Second Law of motion or using the *principle of virtual work*. The former requires the isolation of a typical volume element and the knowledge of all the applied forces. However, for complicated systems—like

constrained systems—the procedure might become exceedingly complicated and unmanageable. For these cases, the principle of virtual work can be a valid alternative.

Consider a displacement field $\boldsymbol{\xi} = \boldsymbol{\xi}(\mathbf{x}, t)$ evolving from an initial time t_i up to a final time t_f. Let $\delta\boldsymbol{\xi}$ be small variation that acts as $\boldsymbol{\xi} \mapsto \boldsymbol{\xi} + \delta\boldsymbol{\xi}$. The principle of virtual work states that: *The solution of the motion is a field $\boldsymbol{\xi}$ such that, for every allowed variation $\delta\boldsymbol{\xi}$, the following equation is satisfied*

$$\int_{t_i}^{t_f} dt\, \delta K - \delta W_I - \delta W_E = 0, \tag{3.10}$$

where an allowed variation has to vanish at the initial final time and must produce a displacement field allowed by the kinematical constraints.

We now discuss each element of the equation. K is the kinetic energy, given by

$$K = \frac{1}{2} \int d^3x\, \rho \dot{\xi}_i \dot{\xi}_i, \tag{3.11}$$

where ρ is the density. δW_I is the infinitesimal work of the internal elastic forces

$$\delta W_I = \int d^3x\, \sigma_{ij} \delta \partial_i \xi_j. \tag{3.12}$$

δW_E is the infinitesimal work of the external forces

$$\delta W_E = -\int d^3x\, f_i^E \delta \xi_i. \tag{3.13}$$

It is crucial to observe that the infinitesimal internal work is expressed as $\sigma_{ij}\delta\partial_i\xi_j$ and not as the variation of an elastic potential energy. This allows the method to be applied even for non-conservative systems. In fact, a non-conservative (odd-elastic) system does not have a potential energy, but still has well defined stresses.

A simple example

Before using it for the plates, we show that the principle of virtual work can be used to derive the standard equations of elasticity. We consider a d-dimensional system with no constraints. Performing the variation of K we get

$$\int_{t_i}^{t_f} dt \int d^dx \left(\rho \dot{\xi}_i \delta \dot{\xi}_i - \sigma_{ij} \delta \partial_i \xi_j + f_i^E \delta \xi_i \right) = 0. \tag{3.14}$$

We then integrate by parts on the time variable for the kinetic term and in space for the internal work. The time boundary terms are dropped because the $\delta\boldsymbol{\xi}$ is vanishing at t_i and t_f, spatial boundary terms are dropped because the the system is infinite and the fields are assumed to be vanishing at infinite

$$\int_{t_i}^{t_f} dt \int d^dx \left(-\rho \ddot{\xi}_i \delta \xi_i + \partial_i \sigma_{ij} \delta \xi_j + f_i^E \delta \xi_i \right) = 0. \tag{3.15}$$

Finally, if the equation holds for *every* $\delta\boldsymbol{\xi}$, then

$$\rho \ddot{\xi}_i = \partial_j \sigma_{ji} + f_i^E. \tag{3.16}$$

3.2.2 Derivation of the equations of motion

We now use the principle of virtual work to derive the equations of motion of the Reissner-Mindlin theory. We assume an external drag force given by $f_i^E = -\Gamma\dot{\xi}_i$. We calculate each term separately. The procedure is similar for all the terms: first we substitute the explicit parametrization in the expression of the three dimensional displacement field, then we integrate over z, assuming a uniform density and finally we integrate by parts, in order to isolate the variations of the fields.

We start from the kinetic term. Substituting the expression for the displacement field of Eqs. (3.2), (3.3) we get

$$\begin{aligned}\int_{t_i}^{t_f} dt\,\delta K &= \int_{t_i}^{t_f} dt \int_V d^3x\,\rho\dot{\xi}_i\delta\dot{\xi}_i \\ &= \int_{t_i}^{t_f} dt \int_V d^3x\,\rho[\dot{\xi}_\alpha\delta\dot{\xi}_\alpha + \dot{w}\delta\dot{w}] \\ &= \int_{t_i}^{t_f} dt \int_V d^3x\,\rho[(\dot{\eta}_\alpha + z\dot{\phi}_\alpha)\delta(\dot{\eta}_\alpha + z\dot{\phi}_\alpha) + \dot{w}\delta\dot{w}]\end{aligned} \tag{3.17}$$

Then we integrate in dz and use

$$\int_{-h/2}^{h/2} dz\,1 = h \qquad \int_{-h/2}^{h/2} dz\,z = 0 \qquad \int_{-h/2}^{h/2} dz\,z^2 = \frac{h^3}{12}, \tag{3.18}$$

obtaining

$$\int_{t_i}^{t_f} dt \int_S d^2x\,\rho[h\dot{\eta}_\alpha\delta\dot{\eta}_\alpha + h\dot{w}\delta\dot{w} + \frac{h^3}{12}\dot{\phi}_\alpha\delta\dot{\phi}_\alpha]. \tag{3.19}$$

Finally, we integrate by parts in time, dropping the boundary terms because the variation vanishes at t_i and t_f

$$\int_{t_i}^{t_f} dt\,\delta K = -\int_{t_i}^{t_f} dt \int_S d^2x\,\rho[h\ddot{\eta}_\alpha\delta\eta_\alpha + h\ddot{w}\delta w + \frac{h^3}{12}\ddot{\phi}_\alpha\delta\phi_\alpha]. \tag{3.20}$$

Then we consider the internal work. As before, we substitute the parametrization of the displacement field

$$\begin{aligned}\int_{t_i}^{t_f} dt\,\delta W_I &= \int_{t_i}^{t_f} dt \int_V d^3x\,\sigma_{ij}\delta u_{ij} \\ &= \int_{t_i}^{t_f} dt \int_V d^3x\,\sigma_{ij}\partial_i\delta\xi_j \\ &= \int_{t_i}^{t_f} dt \int_V d^3x\,[\sigma_{\alpha\beta}(\partial_\alpha\delta\eta_\beta + z\partial_\alpha\delta\phi_\beta) + \sigma_{z\alpha}\delta\phi_\alpha + \sigma_{\alpha z}\partial_\alpha\delta w].\end{aligned} \tag{3.21}$$

Now we have to integrate in dz. Using the definitions of the net stress and moment tensors (3.8) and (3.9) we get

$$\int_{t_i}^{t_f} dt \int_S d^2x \, [N_{\alpha\beta}\partial_\alpha \delta\eta_\beta + M_{\alpha\beta}\partial_\alpha \delta\phi_\beta + N_{z\alpha}\delta\phi_\alpha + N_{\alpha z}\partial_\alpha \delta w]. \tag{3.22}$$

Finally, we integrate by parts in the spatial coordinates. We drop the boundary terms, assuming that the fields go to zero at infinity

$$\int_{t_i}^{t_f} dt \, \delta W_I = \int_{t_i}^{t_f} dt \int_S d^2x \, [-\partial_\alpha N_{\alpha\beta}\delta\eta_\beta - \partial_\alpha M_{\alpha\beta}\delta\phi_\beta + N_{z\alpha}\delta\phi_\alpha - \partial_\alpha N_{\alpha z}\delta w]. \tag{3.23}$$

The last term is the external virtual work. In this case we just have to substitute the parametrization of the displacement field and to integrate in dz, no integration by parts is needed. We get

$$\begin{aligned}
\int_{t_i}^{t_f} dt \, \delta W_E &= \int_{t_i}^{t_f} dt \int_V d^3x \; -\Gamma\dot{\xi}_i\delta\xi_i \\
&= \int_{t_i}^{t_f} dt \int_V d^3x \; -\Gamma[(\eta_\alpha + z\phi_\alpha)(\delta\dot{\eta}_\alpha + z\delta\dot{\phi}_\alpha) + w\delta\dot{w}] \\
&= \int_{t_i}^{t_f} dt \int_S d^2x \; -\Gamma[h\eta_\alpha\delta\dot{\eta}_\alpha + \frac{h^3}{12}\phi_\alpha\delta\dot{\phi}_\alpha + hw\delta\dot{w}] \\
&= \int_{t_i}^{t_f} dt \int_S d^2x \, \Gamma[h\dot{\eta}_\alpha\delta\eta_\alpha + h\dot{w}\delta w + \frac{h^3}{12}\dot{\phi}_\alpha\delta\phi_\alpha].
\end{aligned} \tag{3.24}$$

In the end, we impose (3.10) for all the variations of the plate's fields. Collecting the terms multiplied respectively by $\delta\eta_\alpha, \delta w, \delta\phi_\alpha$, we obtain the equations of motion

$$h(\rho\ddot{\eta}_\alpha + \Gamma\dot{\eta}_\alpha) = \partial_\beta N_{\beta\alpha} \tag{3.25a}$$

$$h(\rho\ddot{w} + \Gamma\dot{w}) = \partial_\alpha N_{\alpha z} \tag{3.25b}$$

$$\frac{h^3}{12}(\rho\ddot{\phi}_\alpha + \Gamma\dot{\phi}_\alpha) = \partial_\beta M_{\beta\alpha} - N_{z\alpha}. \tag{3.25c}$$

These equations of motion cannot be solved without specifying how N and M depend on η, w, ϕ. This will be provided by the constitutive relations.

3.3 Constitutive relations

As we said before, u_{zz} is identically zero. This comes directly from the kinematical assumptions on the allowed displacements. Since $u_{zz} = 0$, the transverse normal stress σ_{zz}, though not zero identically, does not appear in the virtual work statement and, hence, in the equations of motion. Consequently, it amounts to neglecting the transverse normal stress [40]. We thus make the *plane stress*

assumption, in which we assume that the normal stress is identically zero, too. So that

$$\sigma_{zz} = 0. \tag{3.26}$$

We now have a set of allowed strains, that satisfy $u_{zz} = 0$ and a set of allowed stressed, that satisfy $\sigma_{zz} = 0$. The constitutive relations must match these conditions. This requires a reduction procedure of the three dimensional constitutive relations.

In this work, we consider a plate made of a three dimensional material that displays cylindrical isotropy. Its constitutive relations, expressed in the basis of Eq. 1.38, were written in equation 1.63. We further ask for the absence of internal torques. Thus, omitting the basis elements relative to rotations, we have

$$C^{3D}_{ab} = 2 \begin{pmatrix} \frac{3}{2}B & D+H & 0 & 0 & 0 & 0 \\ D-H & \mu_3 & 0 & 0 & 0 & 0 \\ 0 & 0 & \mu_1 & K_1^o & 0 & 0 \\ 0 & 0 & -K_1^o & \mu_1 & 0 & 0 \\ 0 & 0 & 0 & 0 & \mu_2 & K_2^o \\ 0 & 0 & 0 & 0 & -K_2^o & \mu_2 \end{pmatrix}. \tag{3.27}$$

The reduction procedure is the following. We express the elastic tensor in the geometric basis of the plate (Eq. 3.7). We employ this basis because it has an element proportional to the zz entry of the rank-two tensors: P. Then, we invert the matrix and obtain $(C^{3D})^{-1}$, which maps the stresses to the strains with $u = (C^{3D})^{-1}\sigma$. Next, we remove the columns and the rows relative to the basis element P and we get the reduced inverse matrix C^{-1}, which is a 5×5 matrix. By removing the column relative to P, we consider only the strains that induce a plane stress. Removing the row relative to P, we project these strains on the space of the allowed strains. Finally, we re-invert the reduced matrix, ad obtain the plate's elastic tensor: a 5×5 matrix that maps the allowed strains to the allowed stresses.

A simple example We make a simple example in order to make the elastic tensor reduction more intuitive. Consider the following system of two masses connected by springs, anchored to two walls.

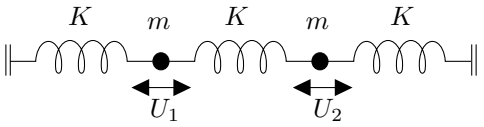

The dependence of the force $F_{1/2}$ applied to the two masses depends on the displacements $U_{1/2}$ according to the relation

$$\begin{pmatrix} F_1 \\ F_2 \end{pmatrix} = K \begin{pmatrix} -2 & 1 \\ 1 & -2 \end{pmatrix} \begin{pmatrix} U_1 \\ U_2 \end{pmatrix}, \tag{3.28}$$

in a more compact form $F = DU$. Then $U = D^{-1}F$, so

$$\begin{pmatrix} U_1 \\ U_2 \end{pmatrix} = \frac{1}{3K} \begin{pmatrix} -2 & -1 \\ -1 & -2 \end{pmatrix} \begin{pmatrix} F_1 \\ F_2 \end{pmatrix}. \tag{3.29}$$

What if we make some hypothesis analogous to the elasticity. Suppose we assume $u_2 = 0$. Then, with the reduction procedure we obtain the reduction $-\frac{2}{3K}F_1 = U_1$, so

$$F_1 = -\frac{3}{2}KU_1. \tag{3.30}$$

Interestingly, this physically corresponds to the following situation.

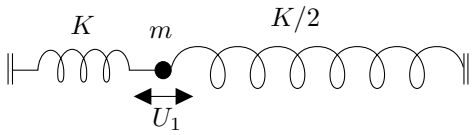

The weak bond $K/2$ arises if we send the mass of the second particle to zero. Thus when we make the hypothesys that $U_2 = 0$ we are actually saying that the energy associated to U_2 is negligible and we assume that U_2 finds a configuration in which the forces at it are zero.

We now apply the reduction procedure to the odd-elastic plate. We note that the only elements of the 3D geometrical basis with a non-zero zz entry are τ^D and τ^{S^1}. These span the same space spanned by D and P of the geometrical basis of the plate. Since that space is invariant under the action of the elastic tensor, we can restrict the reduction procedure to that space; the action of the elastic tensor on the other basis elements will remain unchanged.

The relevant block of the elastic tensor for our reduction procedure is

$$2\begin{pmatrix} \frac{3}{2}B & D+H \\ D-H & \mu_3 \end{pmatrix} \tag{3.31}$$

We express it in the basis $\{D, P\}$ and obtain

$$\begin{pmatrix} \frac{2}{3}(3B - 2\sqrt{2}D + \mu_3) & \sqrt{2}B + \frac{2}{3}(D + 3H - \sqrt{2}\mu_3 \\ \sqrt{2}B + \frac{2}{3}(D - 3H - \sqrt{2}\mu_3) & B + \frac{4}{3}(\sqrt{2}D + \mu_3) \end{pmatrix}. \tag{3.32}$$

Inverting the matrix and get

$$\frac{1}{2}\begin{pmatrix} \frac{3B+4(\sqrt{2}D+\mu_3)}{3(3B\mu_3-2D^2+2H^2)} & \frac{3\sqrt{2}B+2D+6H-2\sqrt{2}\mu_3}{6D^2-6H^2-9B\mu_3} \\ \frac{3\sqrt{2}B+2D-6H-2\sqrt{2}\mu_3}{6D^2-6H^2-9B\mu_3} & -\frac{3B-2\sqrt{2}D+\mu_3}{3D^2-3H^2-9/2B\mu_3} \end{pmatrix}. \tag{3.33}$$

We noe delete the second row and column (relative to the basis element P) and invert the reduced matrix, which is 1×1. We call it $\tilde{B}$: the renormalized bulk modulus

$$\tilde{B} = \frac{3(3B\mu_3 + 2H^2 - 2D^2)}{3B + 4(\sqrt{2}D + \mu_3)}. \tag{3.34}$$

We note that the odd modulus H makes $\tilde{B}$ bigger, and a large value of the passive D could make $\tilde{B}$ negative.

Finally, the whole reduced elastic tensor of the plate, expressed in the plate's geometric basis $\{D, S^1, S^2, T^x, T^y\}$ is

$$C_{ab} = 2\begin{pmatrix} \tilde{B} & 0 & 0 & 0 & 0 \\ 0 & \mu_1 & K_1^o & 0 & 0 \\ 0 & -K_1^o & \mu_1 & 0 & 0 \\ 0 & 0 & 0 & \mu_2 & K_2^o \\ 0 & 0 & 0 & -K_2^o & \mu_2 \end{pmatrix}. \tag{3.35}$$

All the elastic moduli are inherited from the three dimensional constitutive relations. Here, $\tilde{B}$ is a renormalized bulk modulus and maps plane isotropic dilations to the plane isotropic stress. μ_1, μ_2 are passive shear moduli, that map a shear strain to the corresponding shear stress. μ_1 acts on the plane shears S^1, S^2, while μ_2 acts on the transverse shears T^x, T^y. The moduli K_1^o, K_2^o are active and indeed give an antisymmetrical coupling to the shears. K_1^o maps u_{S^1} to σ_{S^2} and u_{S^2} to $-\sigma_{S^1}$. K_2^o does the same on the transverse shears T^x, T^y.

Once we have the constitutive relation, can express the net stress and the moment as functions of the plate's strains. Expressing the strain as $u = u^0 + zu^1$, we note that in a linear system the net stress depends on the 0-order term in z of the strain and the moment depends on the first order.

$$N = \int_{-h/2}^{h/2} dz\, C(u^0 + zu^1) = hCu^0 \tag{3.36}$$

$$M = \int_{-h/2}^{h/2} dz\, zC(u^0 + zu^1) = \frac{h^3}{12} Cu^1. \tag{3.37}$$

Substituting the plate's constitutive relations (3.35) we get

$$\begin{pmatrix} N_D \\ N_{S^1} \\ N_{S^2} \end{pmatrix} = 2h \begin{pmatrix} \tilde{B} & 0 & 0 \\ 0 & \mu_1 & K_1^o \\ 0 & -K_1^o & \mu_1 \end{pmatrix} \begin{pmatrix} u_D^0 \\ u_{S^1}^0 \\ u_{S^2}^0 \end{pmatrix} \tag{3.38a}$$

$$\begin{pmatrix} M_D \\ M_{S^1} \\ M_{S^2} \end{pmatrix} = 2\frac{h^3}{12} \begin{pmatrix} \tilde{B} & 0 & 0 \\ 0 & \mu_1 & K_1^o \\ 0 & -K_1^o & \mu_1 \end{pmatrix} \begin{pmatrix} u_D^1 \\ u_{S^1}^1 \\ u_{S^2}^1 \end{pmatrix} \tag{3.38b}$$

$$\begin{pmatrix} N_{T^x} \\ N_{T^y} \end{pmatrix} = 2h \begin{pmatrix} \mu_2 & K_2^o \\ -K_2^o & \mu_2 \end{pmatrix} \begin{pmatrix} u_{T^x}^0 \\ u_{T^y}^0 \end{pmatrix}. \tag{3.38c}$$

3.4 Odd cycles

With the constitutive relations, we can look at the work of the elastic forces under a closed deformation cycle. Assume that the local strain traces a closed curve in the strain space $\Gamma = \partial\mathcal{S}$ in the strain space. The work per unit surface

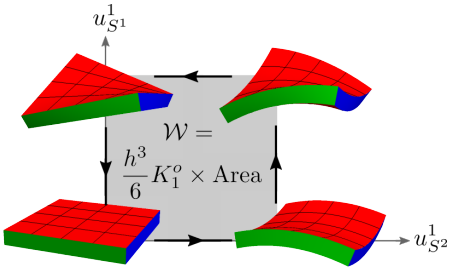

Figure 3.5: A cycle of deformations in the plane $u^1_{S^1}$–$u^1_{S^2}$ of the strain space.

is:

$$\begin{aligned}\mathcal{W} &= \int_{-h/2}^{h/2} dz \oint_\Gamma C_{ab} u_b du_a \\ &= \int_\Gamma h C_{ab} u^0_b du^0_a + \frac{h^3}{12} C_{ab} u^1_b du^1_a \\ &= \int_\mathcal{S} \frac{h}{2} C_{ab} du^0_a \wedge du^0_b + \frac{h^3}{24} C_{ab} du^1_a \wedge du^1_b.\end{aligned} \tag{3.39}$$

The second line follows an integration in dz and the third line follows the application of Stokes' theorem.

We recall that the energy per unit volume extracted over a cycle performed in a fixed plane of the strain space is given by the odd modulus corresponding to the plane times the area encircled by the cycle in the strain space. Here we are looking at the energy extracted per unit surface, which gets a multiplicative factor h when the z-independent strain u^0 is considered and a factor of $\frac{h^3}{12}$ for the z-linear strain u^1. The multiplicative factors have different dimensions because the strain u^0 is a pure number, while u^1 is the inverse of a length.

Considering the constitutive relations of the plate (3.38), there are three independent ways to extract energy with a cycle of deformations, corresponding to the three odd moduli of the constitutive relations.

1. Cycling in the plane $u^0_{S^1}$–$u^0_{S^2}$, the energy density extracted is equal to $2hK^0_1$ times the area enclosed in the strain space. This cycle involves only planar deformations and coincides was already described in Fig. 1.3b.

2. The first "new" cycle is a bending cycle that involves $u^1_{S^1}$ and $u^1_{S^2}$ represented in Fig. 3.5. It extracts $\frac{h^3}{6} K^o_1$ times the area enclosed.

3. A cycle in the $u^0_{T^x}$–$u^0_{T^y}$ plane, the density of work is $2hK^0_1$ times the area enclosed.

We note that the cycle of Fig. 1.3a is not present here because we are considering a system with no internal torques.

3.5 Equations of motion

We can now obtain the explicit equations of motion. Substituting the constitutive relations (3.38) in the general structure of the equations of motion (3.25), we have :

$$\rho\ddot{\eta}_\alpha + \Gamma\dot{\eta}_\alpha = (B\partial_\alpha\partial_\beta + \mu_1\nabla^2\delta_{\alpha\beta} + K_1^o\nabla^2\epsilon_{\alpha\beta})\eta_\beta \tag{3.40a}$$

$$\rho\ddot{w} + \Gamma\dot{w} = \mu_2\nabla^2 w + \mu_2\partial_\alpha\phi_\alpha + K_2^o\epsilon_{\alpha\beta}\partial_\alpha\phi_\beta \tag{3.40b}$$

$$\begin{aligned}\frac{h^2}{12}(\rho\ddot{\phi}_\alpha + \Gamma\dot{\phi}_\alpha) = \frac{h^2}{12}&(B\partial_\alpha\partial_\beta + \mu_1\nabla^2\delta_{\alpha\beta} + K_1^o\nabla^2\epsilon_{\alpha\beta})\phi_\beta \\ &- (\mu_2\delta_{\alpha\beta} + K_2^o\epsilon_{\alpha\beta})(\partial_\beta w + \phi_\beta)\end{aligned} \tag{3.40c}$$

The dynamics of the horizontal displacements η_α is decoupled from the other degrees of freedom. It describes a flat 2D odd-elastic isotropic system without internal torques. This was studied in [12] and reported in section 1.5.

The flexural dynamics desribed by the coupled evolution of w and ϕ_α will be studied in the following chapter.

Chapter 4

Flexural waves

In this chapter we study the flexural dynamics of the plate, described by the evolution of the fields ϕ_x, ϕ_y and w. It regards the deformations that change the orientations of the transverse lines normal to the midplane and the height of the midplane.

In section 1, we discuss the general structure of the normal modes. We show that activity opens a gap in the dispersion relation of the normal modes, allowing for the definition of a topological invariant for the bands. In section 2, we provide an intuition of the effects of activity and a visualization of an an active and a passive normal mode. The topological invariant is analytically computed in the case of a purely active plate. In section 3, an exact mapping between odd-elastic plates and odd-viscous fluids is presented. In section 4, we show that the system displays topologically protected edge modes when the topological invariant is non-zero. We calculate the dispersion profile of the edge modes and present the results of numerical simulations, done for odd-viscous fluids and adapted to odd-elastic plates.

4.1 Normal modes analysis

The flexural dynamics is governed by the following equations

$$\begin{aligned}\frac{h^2}{12}(\rho\ddot{\phi}_\alpha + \Gamma\dot{\phi}_\alpha) &= \frac{h^2}{12}(B\partial_\alpha\partial_\beta + \mu_1\nabla^2\delta_{\alpha\beta} + K_1^o\nabla^2\epsilon_{\alpha\beta})\phi_\beta \\ &\quad - (\mu_2\delta_{\alpha\beta} + K_2^o\epsilon_{\alpha\beta})(\partial_\beta w + \phi_\beta) \\ \rho\ddot{w} + \Gamma\dot{w} &= \mu_2\nabla^2 w + \mu_2\partial_\alpha\phi_\alpha + K_2^o\epsilon_{\alpha\beta}\partial_\alpha\phi_\beta\end{aligned}$$

The equations are linear and we consider plane waves solutions in the form

$$\phi_\alpha(\mathbf{x}, t) = \phi_\alpha e^{i(\mathbf{k}\cdot\mathbf{x}-\omega t)} \qquad w(\mathbf{x}, t) = we^{i(\mathbf{k}\cdot\mathbf{x}-\omega t)}. \tag{4.1}$$

This gives

$$\frac{h^2}{12}(\rho\omega^2 + i\Gamma\omega)\phi_\alpha = \frac{h^2}{12}(Bk_\alpha k_\beta + \mu_1 k^2\delta_{\alpha\beta} + K_1^o k^2\epsilon_{\alpha\beta})\phi_\beta + (\mu_2\delta_{\alpha\beta} + K_2^o\epsilon_{\alpha\beta})(ik_\beta w + \phi_\beta) \tag{4.2}$$

$$(\rho\omega^2 + i\Gamma\omega)w = \mu_2 k^2 w + iK_2^o k_\alpha(\mu_2\delta_{\alpha\beta} + \epsilon_{\alpha\beta})\phi_\beta \tag{4.3}$$

We normalize the wavevector and the vertical displacement with the length scale given by the thickness of the plate and a numerical factor for further convenience

$$\bar{w} = w\frac{\sqrt{12}}{h} \qquad \mathbf{q} = \frac{h}{\sqrt{12}}\mathbf{k} \tag{4.4}$$

that produces

$$\frac{h^2}{12}(\rho\omega^2 + i\Gamma\omega)\phi_\alpha = (Bq_\alpha q_\beta + \mu_1 q^2\delta_{\alpha\beta} + K_1^o q^2\epsilon_{\alpha\beta})\phi_\beta + (\mu_2\delta_{\alpha\beta} + K_2^o\epsilon_{\alpha\beta})(iq_\beta\bar{w} + \phi_\beta) \tag{4.5}$$

$$\frac{h^2}{12}(\rho\omega^2 + i\Gamma\omega)\bar{w} = \mu_2 q^2\bar{w} + iq_\alpha(\mu_2\delta_{\alpha\beta} + K_2^o\epsilon_{\alpha\beta})\phi_\beta. \tag{4.6}$$

In matrix form this is

$$\frac{h^2}{12}(\rho\omega^2 + i\Gamma\omega)\begin{pmatrix}\boldsymbol{\phi}\\ \bar{w}\end{pmatrix} = \mathcal{M}(\mathbf{q})\begin{pmatrix}\boldsymbol{\phi}\\ \bar{w}\end{pmatrix} \tag{4.7}$$

with

$$\mathcal{M}(\mathbf{q}) = \begin{pmatrix} Bq_x^2 + \mu_1 q^2 + \mu_2 & Bq_x q_y + K_1^o q^2 + K_2^o & i(\mu_2 q_x + K_2^o q_y) \\ Bq_x q_y - K_1^o q^2 - K_2^o & Bq_y^2 + \mu_1 q^2 + \mu_2 & i(\mu_2 q_y - K_2^o q_x) \\ -i(\mu_2 q_x - K_2^o q_y) & -i(\mu_2 q_y + K_2^o q_x) & \mu_2 q^2 \end{pmatrix} \tag{4.8}$$

the matrix $\mathcal{M}$ is called *dynamical matrix*. Diagonalizing it, we uncouple the equations of motion: the eigenvectors represent the normal modes: "directions" of oscillation that do not change in time. The eigenvalues define a dispersion relation between ω and $\mathbf{q}$. Let $\lambda(\mathbf{q})$ be an eigenvalue of $\mathcal{M}(\mathbf{q})$, then

$$\frac{h^2}{12}(\rho\omega^2 + i\Gamma\omega) = \lambda(\mathbf{q}). \tag{4.9}$$

We consider a strong drag regime or *overdamped regime*, in which the intertial term is neglected, then the dispersion relation is given by

$$i\omega(\mathbf{q}) = \lambda(\mathbf{q})\frac{12}{\Gamma h^2}. \tag{4.10}$$

We observe that the plate's thickness is factored out of the dynamical matrix. It only affects the frequency of the eigenmodes in a multiplicative way.

The dynamical matrix is simpler in the polar basis. Let

$$\phi_\parallel = \hat{q}_\alpha \phi_\alpha \qquad \phi_\perp = \epsilon_{\alpha\beta}\hat{q}_\alpha \phi_\beta \tag{4.11}$$

be the projections of the vector $\boldsymbol{\phi}$ along and perpendicular to the wavevector $\mathbf{q}$ ($\hat{q}_\alpha = q_\alpha/q$). The *polar basis* $\{\phi_\parallel, \phi_\perp, \bar{w}\}$ is defined by

$$\begin{pmatrix} \phi_\parallel \\ \phi_\perp \\ \bar{w} \end{pmatrix} = \begin{pmatrix} \hat{q}_x & \hat{q}_y & 0 \\ -\hat{q}_y & q_x & 0 \\ 0 & 0 & 1 \end{pmatrix} \begin{pmatrix} \phi_x \\ \phi_y \\ \bar{w} \end{pmatrix} \tag{4.12}$$

and the dynamical matrix in this basis is

$$\mathcal{M}_{\text{polar}} = \begin{pmatrix} (B+\mu_1)q^2 + \mu_2 & K_1^o q^2 + K_2^o & i\mu_2 q \\ -K_1^o q^2 - K_2^o & \mu_1 q^2 + \mu_2 & -iK_2^o q \\ -i\mu_2 q & -iK_2^o q & \mu_2 q^2 \end{pmatrix}. \tag{4.13}$$

The matrix $\mathcal{M}$ is non-Hermitian due to the presence of the active moduli. This causes an anti-hermitian coupling between $\phi_\parallel$ and $\phi_\perp$, proportional to $K_1^o q^2 + K_2^o$ and another anti-hermitian coupling between $\phi_\perp$ and w, proportional to $iK_2^o q$. The matrix depends only on $q = |\mathbf{q}|$, and thus the spectrum too. This is a consequence of cylindrical isotropy in the constitutive relations.

It is easy to verify that the characteristic polynomial $p(\lambda) = \det(\mathcal{M}_{\text{polar}} - \lambda\mathbb{I})$ of the matrix is real

$$\begin{aligned} p(\lambda) = {} & [(B+\mu_1)q^2 + \mu_2 - \lambda](\mu_1 q^2 + \mu_2 - \lambda)(\mu_2 q^2 - \lambda) \\ & - 2(K_1^o q^2 + K_2^o)\mu_2 K_2^o q^2 + [(B+\mu_1)q^2 + \mu_2 - \lambda]K_2^{o\,2} q^2 \\ & - (\mu_1 q^2 + \mu_2 - \lambda)\mu_2^2 q^2 + (K_1^o q^2 + K_2^o)^2(\mu_2 q^2 - \lambda). \end{aligned} \tag{4.14}$$

Then, if λ is an eigenvalue, λ^* is an eigenvalue, too. There are three eigenvalues, so they are either all real or one real and two complex, related by conjugation. Represented in the complex plane as a function of q, they constitute three bands, symmetric under reflection with respect to the real axis.

Passive case

We consider the case of zero activity. When all the odd moduli are set to zero, the dynamical matrix is

$$\mathcal{M}_{\text{polar}} = \begin{pmatrix} (B+\mu_1)q^2 + \mu_2 & 0 & i\mu_2 q \\ 0 & \mu_1 q^2 + \mu_2 & 0 \\ -i\mu_2 q & 0 & \mu_1 q^2 + \mu_2 \end{pmatrix}. \tag{4.15}$$

The matrix is symmetric and has a real spectrum. We immediately recognize an eigenmode oriented as $\phi_\perp$, with eigenvalue $\lambda_1(q) = \mu_1 q^2 + \mu_2$. The other two

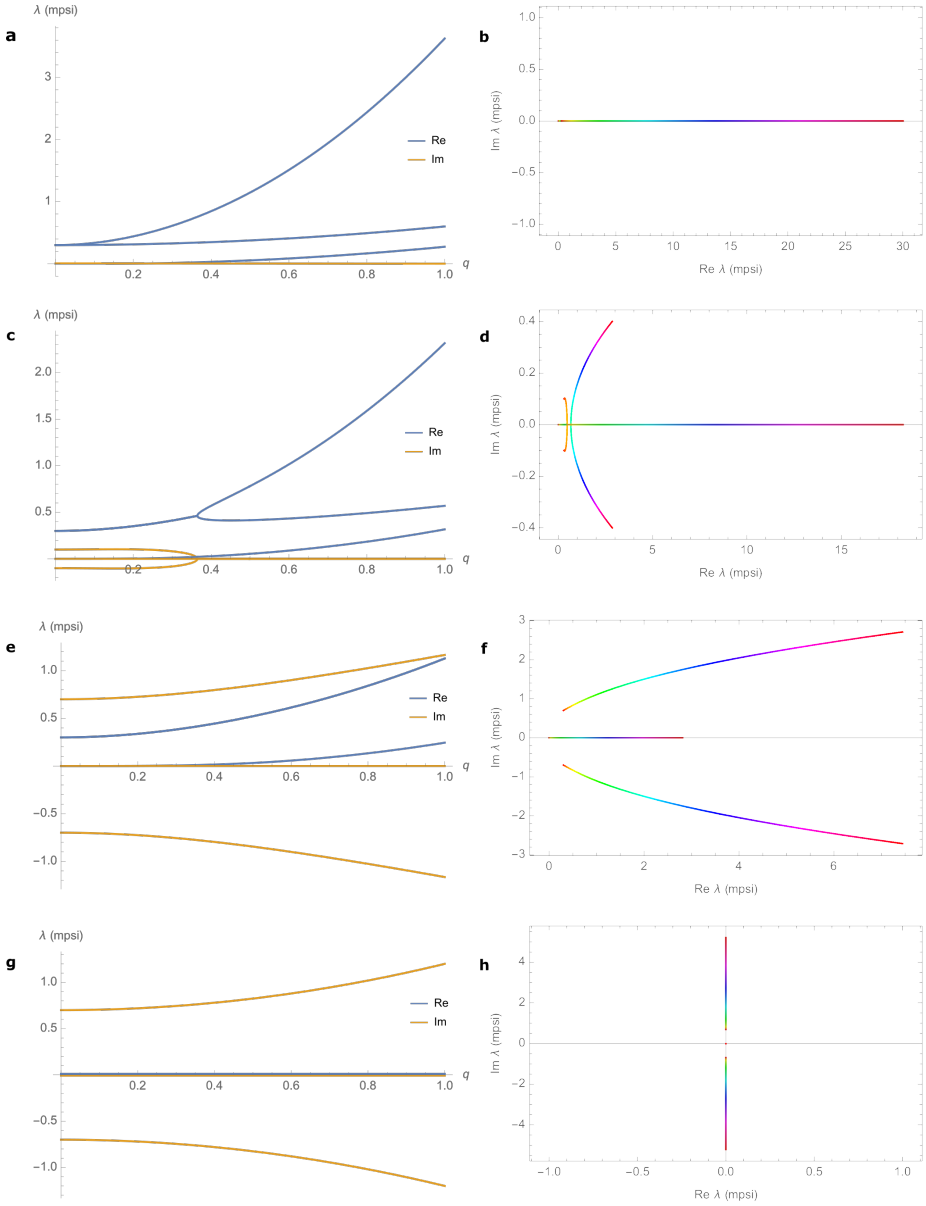

Figure 4.1: Eigenvalues of the dynamical matrix. On the left, we plot separately $\mathrm{Re}\,\lambda(q)$ and $\mathrm{Im}\,\lambda(q)$ for $q \in [0,1]$; at right, the same band-structure is plotted parametrically in the complex plane for $q \in [0,3]$ (red/yellow is $q=0$, violet/red is $q=3$). Elastic moduli and eigenvalues are in mpsi; $1\text{mpsi} = 6.895\text{kN/m}^2$. **(a-b)** Passive case, $B = 1.7, \mu_1 = 0.3, \mu_2 = 0.3, K_1^o = K_2^o = 0$. **(c-d)** Active case with small odd moduli, the spectrum is ungapped $B = 1.7, \mu_1 = 0.3, \mu_2 = 0.3, K_1^o = 0.1, K_2^o = 0.1$. **(e-f)** Active case with large odd moduli, the spectrum is gapped $B = 1, \mu_1 = 0.3, \mu_2 = 0.3, K_1^o = 0.5, K_2^o = 0.7$. **(g-h)** Purely active case, spectrum is imaginary and gapped $B = \mu_1 = \mu_2 = 0, K_1^o = 0.5, K_2^o = 0.7$.

eigenmodes mix the fields $\phi_\parallel$ and w and have the following expressions

$$\lambda_2(q) = \frac{1}{2}\left\{\mu_2 + (B+\mu_1+\mu_2)q^2 + \sqrt{\left[\mu_2 + q^2(B+\mu_1+\mu_2)\right]^2 - 4q^4(B+\mu_1)\mu_2}\right\}$$
$$\lambda_3(q) = \frac{1}{2}\left\{\mu_2 + (B+\mu_1+\mu_2)q^2 - \sqrt{\left[\mu_2 + q^2(B+\mu_1+\mu_2)\right]^2 - 4q^4(B+\mu_1)\mu_2}\right\}. \tag{4.16}$$

We note that $\lambda_1(0) = \lambda_2(0) = \mu_2$ and $\lambda_3(0) = 0$. The $\phi_\perp$ mode produces a finite frequency at infinite wavelength, together the mode identified by λ_2. A plot of $\lambda(q)$ for a passive plate is shown in Fig. 4.1a,b.

Active case

When the active moduli are turned on, the spectrum acquires an imaginary part. If the active moduli are *small* with respect to the passive moduli, the bands can intersect themselves. In figure 4.1c,d we observe for $q \simeq 0.4$ an intersection of two bands; the bands are complex-conjugated before the intersection takes place and both real after the intersection (in panel c we see that both the imaginary parts vanish and that the real parts bifurcate). For higher values of q two bands re-merge, producing a complex-conjugate pair (the second intersection is visible only in the parametric plot, Fig. 4.1d).

We empirically observe that, increasing the odd moduli and lowering the passive moduli, the bands start to lay on different regions of the complex plane (Fig. 4.1e,f); it is possible to draw a curve in the complex plane that does not intersects the spectrum, yet divides the complex plane into two regions. We refer to this situation as a *gapped* band-system

If the passive moduli are set to zero, the spectrum is composed by a vanishing band and two purely imaginary bands. This is the easiest case in which the band-system is gapped and we will study it in detail in the following section.

4.2 Manifestation of activity

In this section we ~~want to~~ provide an intuition of the effects of activity on the plate's dynamics. We focus on two aspects. First, we study the infinite wavelength behaviour of the plate, where the displacement field is homogeneous. Secondly, we expand the analysis to $q \neq 0$, providing a rendering of the deformation and the strain of an active and passive eigenmode.

Infinite wavelength

We study spatially uniform waves setting $q = 0$ in the equations of motion

$$i\frac{\Gamma h^2}{12}\omega \begin{pmatrix}\phi_x\\ \phi_y\\ \bar{w}\end{pmatrix} = \begin{pmatrix}\mu_2 & K_2^o & 0\\ -K_2^o & \mu_2 & 0\\ 0 & 0 & 0\end{pmatrix}\begin{pmatrix}\phi_x\\ \phi_y\\ \bar{w}\end{pmatrix}. \tag{4.17}$$

The eigenvectors of the dynamical matrix are

$$\psi_0 = \begin{pmatrix} 0 \\ 0 \\ 1 \end{pmatrix} \qquad \psi_\pm = \begin{pmatrix} 1 \\ \pm i \\ 0 \end{pmatrix}, \tag{4.18}$$

with eigenvalues $\lambda_0 = 0, \lambda_\pm = \mu_2 \pm iK_2^o$, so that

$$\omega_0 = 0 \qquad i\omega_\pm = \frac{12}{\Gamma h^2}(\mu_2 \pm iK_2^o). \tag{4.19}$$

The vertical oscillation of the plate ψ_0 has zero frequency at infinite wavelength. On the contrary, the oscillation of the angular fields $\psi_\pm$ has a finite frequency. We now study the time evolution of the two angular modes. Let $\tilde{\mu}_2 = \frac{12}{\Gamma h^2}\mu_2$ and $\tilde{K}_2^o = \frac{12}{\Gamma h^2}K_2^o$,

$$\begin{aligned}
\begin{pmatrix} \phi_x \\ \phi_y \end{pmatrix}(x,t) &= \mathrm{Re}\left[\begin{pmatrix} 1 \\ \pm i \end{pmatrix} e^{-(\tilde{\mu}_2 \pm i\tilde{K}_2^o)t}\right] \\
&= e^{-\tilde{\mu}_2 t}\,\mathrm{Re}\left[\begin{pmatrix} e^{\mp i\tilde{K}_2^o t} \\ e^{\mp i\tilde{K}_2^o t \pm i\pi/2} \end{pmatrix}\right] \\
&= e^{-\tilde{\mu}_2 t}\begin{pmatrix} \cos\left(\tilde{K}_2^o t\right) \\ \cos\left(\mp\tilde{K}_2^o t \pm \pi/2\right) \end{pmatrix} \\
&= e^{-\tilde{\mu}_2 t}\begin{pmatrix} \cos\left(\tilde{K}_2^o t\right) \\ \cos\left(\tilde{K}_2^o t - \pi/2\right) \end{pmatrix} \\
&= e^{-\tilde{\mu}_2 t}\begin{pmatrix} \cos\left(\tilde{K}_2^o t\right) \\ \sin\left(\tilde{K}_2^o t\right) \end{pmatrix}.
\end{aligned} \tag{4.20}$$

The two modes $\psi_\pm$ display the same behaviour: the vector $\boldsymbol{\phi}$ rotates in the x-y plane, while being exponentially damped. The attenuation rate is proportional to the passive modulus μ_2—this is the typical effect of the strong drag on passive systems. Since the wave is spatially uniform, all the derivative terms in the expression for the strain (3.4) are equal to zero and the only non-zero strain component is the transverse strain, which is proportional to the vector $\boldsymbol{\phi}$, $u_{\alpha z} = \phi_\alpha/2$. The rotation of the vector $\boldsymbol{\phi}$ traces an active cycle that extracts energy in order to balance the dissipation led by the drag (proportional to Γ).

Active vs. passive mode comparison In Fig. 4.2 we show two renderings of an active and a passive eigenmodes. When q is finite, the deformation involves both the vertical displacement and the angular fields, because the dynamical matrix is not block diagonal anymore. The passive mode is obtained from a dynamical matrix that has $B = 1, \mu_1 = 0.3, \mu_2 = 0.3$ and vanishing odd moduli $K_1^o = K_2^o = 0$. The active mode is realized only with K_2^o: $B = 0, \mu_1 = 0, \mu_2 =$

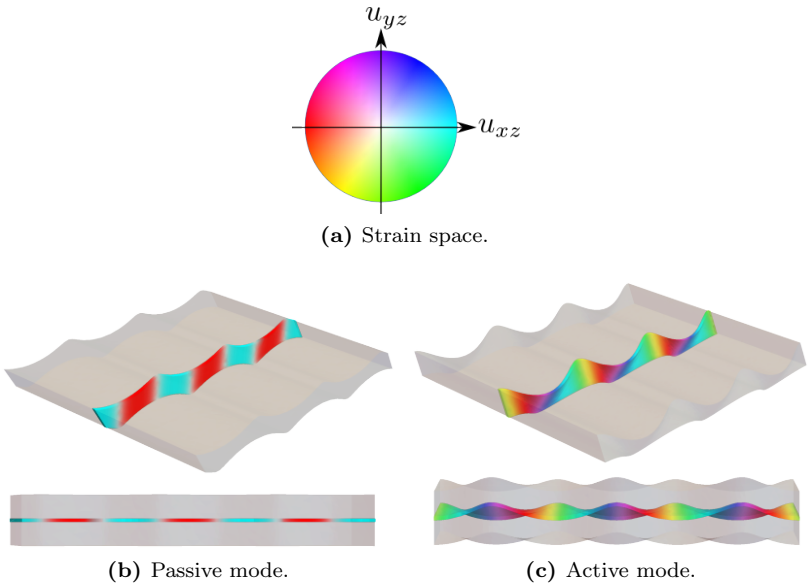

(a) Strain space.

(b) Passive mode.

(c) Active mode.

Figure 4.2: Perspective and top view of bulk flexural eigenmodes.

$0, K_1^o = 0, K_2^o = 1$. We colour a slice of the plate according to the local transverse strain. The tone of the colour depends on the direction of the strain in the plane u_{xz}-u_{yz}, while the opacity is proportional to the norm $\sqrt{(u_{xz})^2 + (u_{yz})^2}$.

We observe that the passive mode oscillates along a straight line in the strain space, passing periodically through the origin (zero opacity). On the contrary, the active mode carries out a circle in the strain space: the slice changes colour without loss of opacity. The energy extracted along the circle, proportional to the area covered in the strain plane, allows the propagation of the wave in time.

The eigenmodes of a passive plate necessarily trace straight lines in the strain space. In fact, from (4.15), any passive plate has a mode that involves only $\phi_\perp$, in which $\boldsymbol{\phi}$ oscillates in a direction orthogonal to the wavevector $\mathbf{q}$. For that eigenmode $w = 0$, and $u_{\alpha z} = \frac{1}{2}(\partial_\alpha w + \phi_\alpha) = \frac{1}{2}\phi_\alpha$. Thus, the transverse strain $u_{\alpha z}$ oscillates in the direction perpendicular to $\mathbf{q}$, together with ϕ_α. The other two modes couple $\phi_\parallel$ and w. The strain component perpendicular to $\mathbf{q}$ is identically zero, because here $\phi_\perp = 0$ and $\nabla_\perp w = 0$. These two modes then oscillate parallel to $\mathbf{q}$ and trace a straight line in the strain space. When K_2^o is turned on, it provides an odd coupling between $\phi_\perp$ and $\phi_\parallel$ and causes the "rotation" of the eigenmodes in the strain space.

4.3 The topological invariant

consider?

We set ourselves to the purely active case, in which the passive moduli B, μ_1, μ_2 are set to zero. Then

$$\mathcal{M}(\mathbf{q}) = \begin{pmatrix} 0 & K_1^o q^2 + K_2^o & iK_2^o q_y \\ -K_1^o q^2 - K_2^o & 0 & -iK_2^o q_x \\ iK_2^o q_y & -iK_2^o q_x & 0 \end{pmatrix} \tag{4.21}$$

and the spectrum is

$$\lambda_0(q) = 0 \qquad \lambda_\pm(q) = \pm i\sqrt{(K_2^o q)^2 + (K_1^o q^2 + K_2^o)^2}. \tag{4.22}$$

The opening of the gap is regulated by K_2^o. We assume $K_2^o \neq 0$, and define

$$\gamma := \frac{K_1^o}{K_2^o}; \tag{4.23}$$

this allows us to write the dynamical matrix as

$$\mathcal{M}(\mathbf{q}) = iK_2^o \begin{pmatrix} 0 & -i(\gamma q^2 + 1) & q_y \\ i(\gamma q^2 + 1) & 0 & -q_x \\ q_y & -q_x & 0 \end{pmatrix}. \tag{4.24}$$

The matrix structure is thus controlled uniquely by γ. We write the last matrix as a linear combination of the matrices

$$S_x = \begin{pmatrix} 0 & 0 & 0 \\ 0 & 0 & -1 \\ 0 & -1 & 0 \end{pmatrix} \quad S_y = \begin{pmatrix} 0 & 0 & 1 \\ 0 & 0 & 0 \\ 1 & 0 & 0 \end{pmatrix} \quad S_z = \begin{pmatrix} 0 & -i & 0 \\ i & 0 & 0 \\ 0 & 0 & 0 \end{pmatrix}, \tag{4.25}$$

so that

$$\mathcal{M}(\mathbf{q}) = iK_2^o \vec{M}(\mathbf{q}) \cdot \vec{S} \tag{4.26}$$

with

$$\vec{M}(\mathbf{q}) = \begin{pmatrix} q_x \\ q_y \\ \gamma q^2 + 1 \end{pmatrix} \tag{4.27}$$

and $\vec{S} = (S_x, S_y, S_z)$. In the end, we define the typical active frequency $\omega^o = \frac{12K_2^o}{\Gamma h^2}$ so that the wave equation assumes the form of an eigenvalue problem for a hermitian matrix

$$\omega \begin{pmatrix} \boldsymbol{\phi} \\ \bar{w} \end{pmatrix} = \omega^o \left(\vec{M}(\mathbf{q}) \cdot \vec{S} \right) \begin{pmatrix} \boldsymbol{\phi} \\ \bar{w} \end{pmatrix}. \tag{4.28}$$

$\{S_i\}$ is a set of hermitian traceless matrices that satisfy the commutation relations $[S_i, S_j] = i\epsilon_{ijk} S_k$ of $\mathfrak{su}(2)$. The eigenvalues of $\vec{M} \cdot \vec{S}$ are

$$\omega/\omega^o = \left\{ 0, \pm\sqrt{M_x^2 + M_y^2 + M_z^2} \right\} = \{0, \pm\sqrt{q^2 + (\gamma q^2 + 1)^2}\}. \tag{4.29}$$

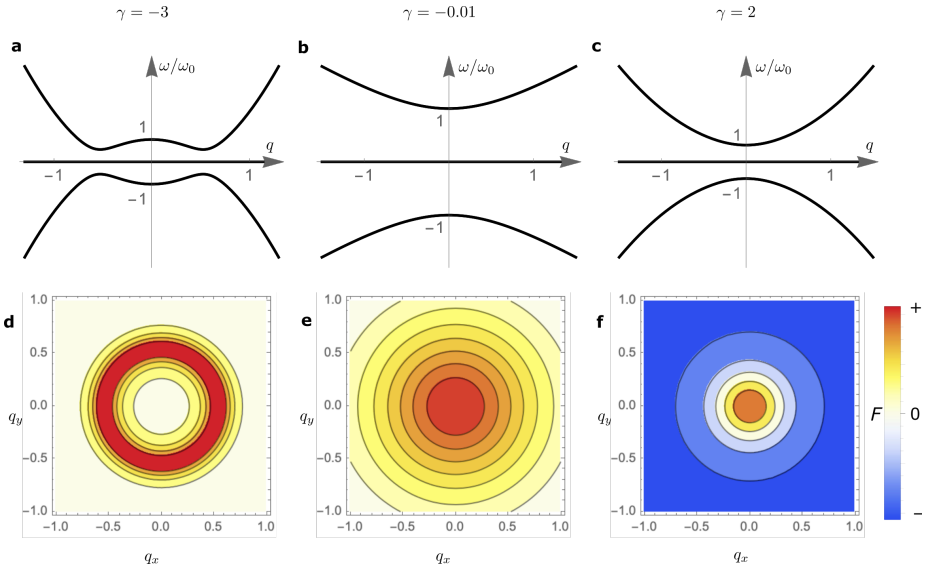

Figure 4.3: Imaginary spectrum (a-c) and Berry curvature (d-f) when the passive moduli vanish. The spectrum has an open gap if $K_2^o \neq 0$. In **a,d**, $\gamma = -3$. The non-zero bands have a mexican-hat shape and the curvaure is concentrated along an annulus. In **b**, **e**, $\gamma = -0.01$, thus the the bands have only one local extremum and the Berry curvature is concentrated at $q = 0$. In **c**, **f**, $\gamma = 2$, the spectrum bands have one local extremum and the curvature has no defined sign, giving a zero Chern number.

The bands have a Mexican-hat shape if $\gamma < -1/2$, otherwise they have a parabolic shape, with a minimum at $q = 0$ (Fig. 4.3).

The hermitian matrix $\vec{M}(\mathbf{q}) \cdot \vec{S}$ can be considered a Bloch Hamiltonian over the space of wave-vectors, the *momentum space*, which is $\mathbb{R}^2$. The eigenvectors then define a vector bundle over such manifold. Since $\mathbb{R}^2$ is contractible, the bundle is necessarily trivial. However, we will see that in this case $\mathbb{R}^2$ can be effectively compactified to a sphere, which can be the base manifold of a non-trivial bundle.

First of all we have to notice that a multiplicative factor does not affect the eigenvectors so we can divide the Hamiltonian by $||\vec{M}||$, which is always non-zero, and focus on

$$\mathcal{N}(\mathbf{q}) = \hat{n}(\mathbf{q}) \cdot \vec{S}, \tag{4.30}$$

with $\hat{n} = \vec{M}/||\vec{M}||$. This Hamiltonian has the same eigenvectors of $\mathcal{M}(\mathbf{q})$.

We stress that $\vec{M} : \mathbb{R}^2 \to \mathbb{R}^3$, while $\hat{n} : \mathbb{R}^2 \to S^2$. The explicit expression for $\hat{n}$ is:

$$\hat{n}(\mathbf{q}) = \frac{1}{\sqrt{q^2 + (1 + \gamma q^2)^2}} \begin{pmatrix} q_x \\ q_y \\ \gamma q^2 + 1 \end{pmatrix} \tag{4.31}$$

Then, if $\gamma \neq 0$, which means $K_1^o \neq 0$, $\lim_{\mathbf{q}\to\infty} \hat{n}$ does not depend on the chosen direction. Identifying all the points that lay at infinity, we compactify the momentum space to a sphere, which we call $\mathcal{B}$. In this case, the Chern number becomes a well defined topological invariant and the eigenmodes can describe a non-trivial bundle over the momentum space.

We now calculate the Berry curvature F of the eigenmodes. We define the function

$$\begin{aligned} \mathscr{S} : S^2 &\to \text{Hermit}_3 \\ \hat{v} &\mapsto \hat{v} \cdot \vec{S}, \end{aligned} \tag{4.32}$$

that is a Hamiltonian over the sphere S^2. Our Hamiltonian $\mathcal{N}$ can be re-written as $\mathcal{N} = \mathscr{S} \circ \hat{n}$, i.e.

$$\mathcal{N} : \mathbb{R}^2 \xrightarrow{\hat{n}} S^2 \xrightarrow{\mathscr{S}} \text{Hermit}_3. \tag{4.33}$$

We see that $\mathcal{N}$ is the pullback through $\hat{n}$ of $\mathscr{S}$. Hence, the Berry curvature induced by the eigenmodes of $\mathcal{N}$ on $\mathbb{R}^2$ is equal to the pull-back through $\hat{n}$ of the Berry curvature F^{S^2} induced on the sphere by the bands of $\mathscr{S}$.

$$F = \hat{n}^* F^{S^2} \tag{4.34}$$

The first Chern number can be calculated exploiting the pullback:

$$\mathcal{C} = \frac{1}{2\pi} \int_{\mathbb{R}^2} \hat{n}^* F^{S^2}. \tag{4.35}$$

Berry curvature on the sphere In order to calculate the Berry curvature of the sphere induced by $\mathscr{S}$, we calculate the eigenvectors of $\hat{n} \cdot \vec{S}$. We exploit the fact that $\vec{S}$ is a spin 1 representation of $\mathfrak{su}(2)$. Let $\hat{n} = (\sin\theta\cos\phi, \sin\theta\sin\phi, \cos\theta)$

be an arbitrary unit vector and $\hat{z} = (0, 0, 1)$ the unit vector along the z axis. Let R be a rotation such that $\hat{n} = R\hat{z}$ and D the representation of rotations that satisfies

$$D^{-1} S_i D = R_{ij} S_j. \tag{4.36}$$

This allows to express $\hat{n} \cdot \vec{S}$ as

$$\begin{aligned} \hat{n} \cdot \vec{S} &= (R\hat{z}) \cdot \vec{S} \\ &= \hat{z} \cdot (R^\top \vec{S}) \\ &= R^\top_{zj} S_j \\ &= D S_z D^{-1}. \end{aligned} \tag{4.37}$$

Then, if $\psi(\hat{z})$ is an eigenvector of S_z, $\psi(\hat{n}) = D\psi(\hat{z})$ is an eigenvector of $\hat{n} \cdot \vec{S}$.

We now use the precise rotation and the corresponding representation to calculate the eigenvectors of $\hat{n} \cdot \vec{S}$. We denote $R_v(\alpha)$ the counterclockwise rotation around the axis $\hat{v}$ of angle α and $D_v(\alpha) = \exp\left(-i\alpha\, \hat{v} \cdot \vec{S}\right)$ is its spin representation. We have

$$\hat{n} = R_z(\phi) R_y(\theta) \hat{z}. \tag{4.38}$$

The eigenvectors of S_z are

$$\psi_0(\hat{z}) = \begin{pmatrix} 0 \\ 0 \\ 1 \end{pmatrix} \qquad \psi_\pm(\hat{z}) = \frac{1}{\sqrt{2}} \begin{pmatrix} 1 \\ \pm i \\ 0 \end{pmatrix} \tag{4.39}$$

with eigenvalues $\{0, \pm 1\}$. The eigenvectors $\psi(\hat{n}) = D_z(\phi) D_y(\theta) \psi(\hat{z})$ are

$$\begin{aligned} \psi_0(\hat{n}) &= \begin{pmatrix} -i \cos\theta \sin\theta \\ -i \sin\theta \sin\theta \\ \cos\theta \end{pmatrix} \\ \psi_\pm(\hat{n}) &= \frac{1}{\sqrt{2}} \begin{pmatrix} \cos\theta \cos\phi \mp i \sin\theta \\ \pm i \cos\phi + \cos\theta \sin\phi \\ -i \sin\theta \end{pmatrix}. \end{aligned} \tag{4.40}$$

We calculate the expression of the Berry connection by its definition (2.9) and obtain $A^{S^2}_\pm = \pm \cos\theta \, d\phi$ and $A^{S^2}_0 = 0$. The Berry connection $F = dA$ is then

$$F^{S^2}_0 = 0 \qquad F^{S^2}_\pm = \mp \sin\theta \, d\theta \wedge d\phi. \tag{4.41}$$

We notice that $F^{S^2}_-$ is the volume form of the sphere, so that $\int_{S^2} F^{S^2}_- = 4\pi$. The measure of the North or South hemisphere $H_{N/S}$ is $\int_{H_{N/S}} F^{S^2}_- = 2\pi$.

Calculation of the Chern number Now we can discuss the integral of Eq. (4.35). Depending on the behaviour of $\hat{n}$, the pullback is performed differently and gives different results.

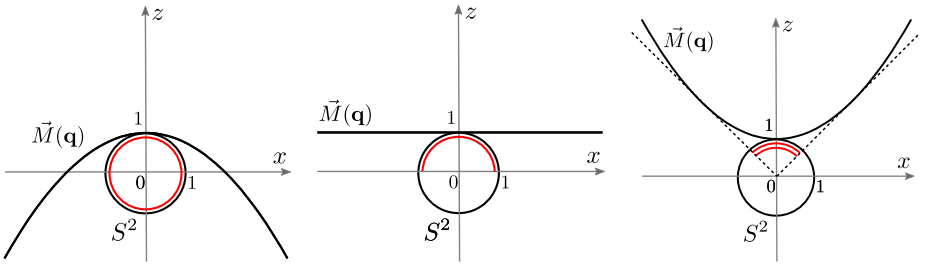

(a) $\gamma < 0$. **(b)** $\gamma = 0$. **(c)** $\gamma > 0$.

Figure 4.4: A section of $\vec{M}(\mathbf{q})$ and of the unit sphere in the (x, z)-plane. In red, the projection on the unit sphere. The behaviour of the map $\hat{n}$ can be understood visualizing the map $\vec{M}$ of Eq. 4.27. **(a)** $\vec{M}$ describes a paraboloid that encloses the origin, then $\hat{n} = \vec{M}/||\vec{M}||$ covers the whole unit sphere. **(b)** $\vec{M}$ describes a horizontal plane, whose projection on the unit sphere covers the North hemisphere. **(c)** $\vec{M}$ describes a paraboloid pointing upwards. Then, $\hat{n}$ covers the same portion of the unit sphere two times, with opposite orientation.

$\gamma < 0$ The map $\hat{n} : \mathbb{R}^2 \to S^2$ is injective and covers the whole sphere—apart from the South pole, which has measure zero. Then $\hat{n}(\mathbb{R}^2) = S^2$ and the integral in (4.35) can be pushed to the sphere, so that

$$\mathcal{C}_- = \frac{1}{2\pi} \int_{S^2} F^{S^2} = 2 \tag{4.42}$$

$\gamma = 0$ The map $\hat{n}$ is injective and covers the north Hemisphere: $\hat{n}(\mathbb{R}^2) = H_N$. Pushing the integral to the sphere, we obtain

$$\mathcal{C}_- = \frac{1}{2\pi} \int_{H_N} F^{S^2} = 1. \tag{4.43}$$

$\gamma > 0$ The map $\hat{n}$ covers the same portion U of the unit sphere two times, with opposite orientation. The two contributions are opposite and give

$$\mathcal{C}_- = \frac{1}{2\pi} \left(\int_U F^{S^2} - \int_U F^{S^2} \right) = 0. \tag{4.44}$$

The explicit form of F can be obtained noting that the Berry curvature on the sphere can be expressed as

$$F_\pm^{S^2} = \mp \frac{1}{2} \epsilon^{ijk} n_i \, dn_j \wedge dn_k \tag{4.45}$$

where $\hat{n} = (\sin\theta\cos\phi, \sin\theta\sin\phi, \cos\theta)$. Then substituting $n_i = M_i(\mathbf{k})/||\vec{M}(\mathbf{k})||$, we obtain:

$$F_\pm(\mathbf{q}) = \mp \frac{\vec{M}}{|\vec{M}|^3} \cdot \left(\frac{\partial \vec{M}}{\partial q_x} \times \frac{\partial \vec{M}}{\partial q_y} \right) dq_x \wedge dq_y. \tag{4.46}$$

Substituting the expression for $\vec{M}(\mathbf{k})$ given by Eq. 4.27 we end up with:

$$F_{\pm}(\mathbf{q}) = \mp \frac{1-\gamma q^2}{[q^2+(\gamma q^2+1)^2]^{3/2}} dq_x \wedge dq_y \tag{4.47}$$

The Berry curvature has a fixed sign if $\gamma < 0$, i.e. if the odd moduli have opposite sign. If $\gamma < -1/4$, it is concentrated along an annulus at finite q, while for $-1/4 < \gamma < 0$ it concentrates at the origin of the momentum space $q = 0$. When the odd moduli have the same sign, the Berry curvature of each band has not a defined sign anymore, and indeed its integral gives a zero Chern number (Fig 4.3 d-f).

4.4 Mapping to odd viscosity

The equations that govern the flexural waves in an overdamped active plate are incredibly close to the ones that describe an odd-viscous fluid. The topological properties of the latter have been first investigated Delplace et al. in [22] in the context of equatorial waves and a generalization to odd viscous fluids was done by Souslov et al. in [21]. There, the physical fields are the density ρ and the velocity $\mathbf{v}$. The parameters are the average density ρ_0, a typical frequency ω_B analoguous to the cyclotron frequency, the viscosity ν, odd viscosity ν^0 and the speed of sound c. The linearized equations for a two-dimensional odd-viscous fluid are

$$\begin{aligned} \partial_t \rho(\mathbf{r},t) &= -\rho_0 \nabla \cdot \mathbf{v}(\mathbf{r},t) \\ \partial_t \mathbf{v} &= -c^2 \nabla \rho/\rho_0 + \omega_B \mathbf{v}^* + \nu \nabla^2 \mathbf{v} + \nu^o \nabla^2 \mathbf{v}^*, \end{aligned} \tag{4.48}$$

where $\mathbf{v}^* \equiv (v_y, -v_x)$ is the velocity rotated by 90°. Plane waves proportional to $e^{i(\mathbf{kx}-\omega t)}$ are studied. The following dimensionless variables are defined: $\bar{\rho} = \rho/\rho_0, \bar{\mathbf{v}} = \mathbf{v}/c, \bar{\omega} = \omega/\omega_B, \mathbf{q} = \mathbf{k}c/\omega_B, m = \omega_B \nu/c^2, m^o = \omega_B \nu^o/c^2$. Then the dimensionless equations for the waves are

$$\bar{\omega} \begin{pmatrix} \bar{\rho} \\ \bar{v}_x \\ \bar{v}_y \end{pmatrix} = \begin{pmatrix} 0 & q_x & q_y \\ q_x & -imq^2 & -i(1-m^o q^2) \\ q_y & i(1-m^o q^2) & -imq^2 \end{pmatrix} \begin{pmatrix} \bar{\rho} \\ \bar{v}_x \\ \bar{v}_y \end{pmatrix}. \tag{4.49}$$

We compare these equations with the equations of flexural waves for an active plate with $B = \mu_2 = 0$. We define the dimensionless variables $\bar{\omega} = \omega/\omega_0$, $\bar{\mu}_1 = \mu_1/K_2^o$. We recall the definitions of $\bar{w} = w\frac{\sqrt{12}}{h}$, $\mathbf{q} = \mathbf{k}\frac{h}{\sqrt{12}}$, $\gamma^o = K_1^o/K_2^o$ and the typical active frequency $\omega^o = \frac{12K_2^o}{\Gamma h^2}$. Then

$$\bar{\omega} \begin{pmatrix} \phi_x \\ \phi_y \\ \bar{w} \end{pmatrix} = \begin{pmatrix} -i\bar{\mu}_1 q^2 & -i(1+\gamma^o q^2) & q_y \\ i(1+\gamma^o q^2) & -i\bar{\mu}_1 q^2 & -q_x \\ q_y & -q_x & 0 \end{pmatrix} \begin{pmatrix} \phi_x \\ \phi_y \\ \bar{w} \end{pmatrix} \tag{4.50}$$

If we identify $\bar{\mu}_1 \leftrightarrow m$ and $\gamma^o \leftrightarrow -m^o$, the two matrices are similar. The explicit

mapping is given by

$$\begin{pmatrix} \bar{\rho} \\ v_x \\ v_y \end{pmatrix} \leftrightarrow \begin{pmatrix} 0 & 0 & 1 \\ 0 & -1 & 0 \\ 1 & 0 & 0 \end{pmatrix} \begin{pmatrix} \phi_x \\ \phi_y \\ \bar{w} \end{pmatrix}, \tag{4.51}$$

thus

$$\bar{w} \leftrightarrow \bar{\rho} \qquad \phi_x \leftrightarrow \bar{v}_y \qquad \phi_y \leftrightarrow -\bar{v}_x. \tag{4.52}$$

Hence the results obtained for odd-viscous systems can be mapped to odd-elastic plates.

4.5 Edge modes

In this section we discuss the existence of edge modes for a purely active plate in the overdamped regime. Following [21], we estimate the penetration depth and the profile of the edge waves. We then present the numerical simulations on odd viscosity done in [21], which we adapt to odd-elastic plates through the exact mapping.

As we discussed in section 2.5, the first Chern number is related to the existence of edge modes. The frequency bands are gapped in the bulk, meaning that no wave with frequency in the gap can propagate there. When the first Chern number is non-zero, chiral edge modes propagate at the boundaries of the system with frequencies in the band gap. The principle of bulk-edge correspondence tells us that the expected net number of edge states at an interface between two systems L and R with invariants $\mathcal{C}^{\mathrm{L/R}}$ is $N = \mathcal{C}_-^{\mathrm{L}} - \mathcal{C}_-^{\mathrm{R}}$ [21].

Profile of the edge modes We consider a purely active plate. Its frequency bands are given by

$$\omega_\pm = \pm\omega_0\sqrt{q^2 + (\gamma q^2 + 1)^2}. \tag{4.53}$$

The edge modes can be studied from the spectrum equation (4.53). We consider the simplified geometry of a semi-infinite plate in the upper (x, y)-half-plane, i.e. $\{(x, y) \in \mathbb{R}^2 \mid y > 0\} = \mathbb{R} \times \mathbb{R}_+$. We look for solutions of the form $\exp\{i[q_x\bar{x} + (q_y + i\kappa)\bar{y} - \omega t]\}$, where $\bar{x} = x\sqrt{12}/h$ and $\bar{y} = y\sqrt{12}/h$ are the dimensionless spatial coordinates. The penetration depth is given by κ^{-1}, and must be positive. The wave is exponentially damped for $y \to +\infty$. We study edge modes that propagate along the interface with a long wavelength, thus we assume $q_x = 0$. Since the edge modes are usually non-gapped, we impose $\omega(q_x = 0) = 0$ in the dispersion relation, obtaining:

$$(q_y + i\kappa)^2 + \left[1 + \gamma(q_y + i\kappa)^2\right]^2 = 0, \tag{4.54}$$

that has solutions:

$$q_y + i\kappa = \frac{\pm i \pm \sqrt{-1 - 4\gamma}}{2\gamma}. \tag{4.55}$$

We distinguish two cases, in which the square root behaves differently

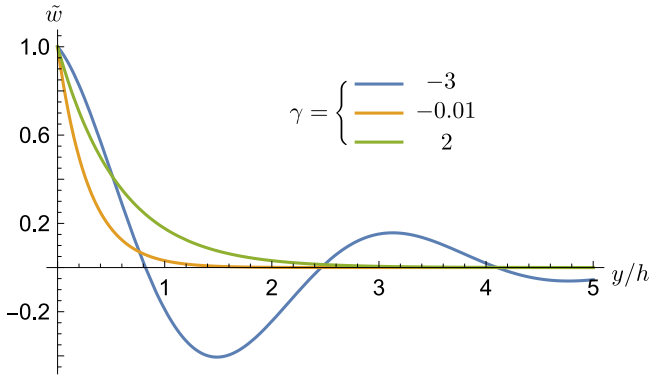

Figure 4.5: Penetration of the edge modes. For $-1/4 < \gamma < 0$ the mode is purely damped. For $\gamma < -1/4$ the mode oscillates while being damped. For $\gamma > 0$ there are still edge modes, but they are not topologically protected anymore.

$\gamma > -1/4$ The acceptable solutions (with positive κ) are:

$$q_y = 0 \quad \kappa_\pm = \frac{\pm 1 + \sqrt{1+4\gamma}}{2\gamma} \tag{4.56}$$

meaning that there are two edge modes, both purely damped in the y direction.

In the limit of $\gamma \to 0$ ($K_1^o \to 0$), κ goes to $\{+\infty, 1\}$, thus $\kappa_\pm^{-1} \to \{0, 1\}$. One mode has a vanishing penetration depth, thus it does not allow a hydrodynamic description. Only the other mode is observable.

If $\gamma \to +\infty$, κ^{-1} decays as $1/\sqrt{\gamma}$ for both the modes. When K_2^o vanishes compared to K_1^o, the penetration depth diverges and the edge modes fully propagate in the bulk.

$\gamma < -1/4$ Both damping ad wave propagation are displayed

$$q_y = \pm\frac{\sqrt{-1-4\gamma}}{2\gamma} \quad \kappa = \frac{1}{2|\gamma|} \tag{4.57}$$

The profile of the edge mode necessarily decays and oscillates away from the edge (blue line in Fig. 4.5)

In the limit for $\gamma \to -\infty$, $q_y \to 1/\sqrt{|\gamma|}$ and $\kappa = 1/(2|\gamma|)$. The typical lengths of damping and oscillation both grow.

We have predicted the profile of the edge modes for all the values of $\gamma = K_1^o/K_2^o$. The propagation of the modes is topologically protected only when the bulk Chern number is non-zero i.e. if $\gamma < 0$. This is shown by numerical simulations.

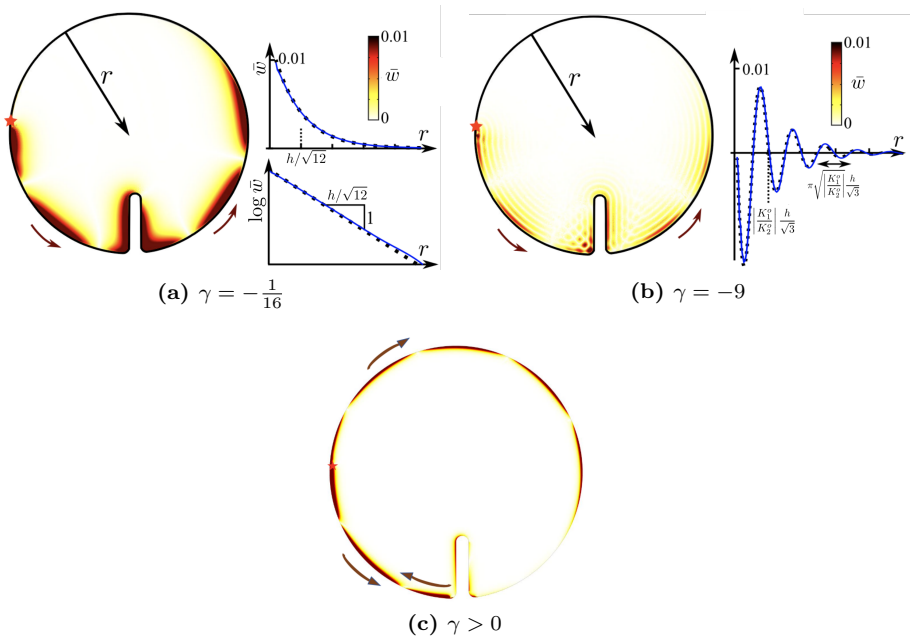

(a) $\gamma = -\frac{1}{16}$ **(b)** $\gamma = -9$

(c) $\gamma > 0$

Figure 4.6: Simulations showing edge states adapted from [21]. A source that produces a perturbation with frequency in the band gap is indicated by the red star. **(a)** A negative small value of $\gamma = K_1^o/K_2^o$ allows the propagation of a unidirectional edge mode that surpasses the obstacle without back-scattering. The profile of the mode is shown in linear- and log-scale, showing agreement with theoretical predictions. **(b)** A large negative value of γ allows the propagation of a topologically-protected mode with a oscillating profile. The profile of the mode is in agreement with the predictions. **(c)** When $\gamma > 0$, topological protection is loss and two modes propagate away from the source in opposite directions. Back-scattering on the obstacle is observed.

Numerical simulations We adapt the results of the simulations made by Souslov et al. [21] with COMSOL Multiphysics software, through the exact mapping to odd-elasticity. To all extents, these describe an odd-elastic plate in the overdamped regime with the passive moduli set to zero.

The plate has a keyhole shape (Fig. 4.6) and is supposed to be confined by a hard wall. The boundary conditions are $\boldsymbol{\phi} \cdot \hat{n} = 0$, where $\hat{n}$ is the unit vector normal to the boundary, in combination with zero force perpendicular to $\hat{n}$. A small source with frequency in the gap is located at a point of the boundary.

The wave originated from the source propagates along the boundaries of the system, without diffusion in the bulk. When $\gamma < 0$, i.e. if K_1^o and K_2^o have opposite signs, the Chern number is non-zero and the perturbation propagates unidirectionally, with direction set by K_2^o. The wave surpasses the obstacle without back-scattering, showing topological protection (Fig. 4.6(a-b)). Vice-

versa, if $\gamma > 0$, i.e. if the two odd moduli have the same sign, the bulk is topologically trivial and the modes are not topologically protected. Two modes propagate away from the source in opposite directions and when one encounters the obstacle a portion of the wave is back-scattered (Fig. 4.6c).

The radial profiles of the edge modes are verified to be in agreement with the theoretical predictions. For low γ, the wave is exponentially damped, with typical length $h/\sqrt{12}$ ($\kappa^{-1} = 1$ in dimensionless units) (Fig. 4.6a). For large (negative) values of γ, the profile of the wave oscillates while being damped. The wavelength is $2\pi/q_y \simeq 2\pi\sqrt{|\gamma|}h/\sqrt{12}$, the penetration depth is $2|\gamma|h/\sqrt{12}$.

4.5.1 Effects of the passive moduli

When the passive moduli are turned on, the dynamical matrix $\mathcal{M}$ obtains an hermitian part. Vice-versa, the Hamiltonian $\frac{1}{i}\mathcal{M}$ is Hermitian in the purely active case and gets an anti-hermitian component when passive moduli are present.

Small passive coefficients continuously deform the band structure, as we showed in Fig. 4.1. There are still three-well defined bands with no crossing, so that the spectrum remains gapped. The $\mu_1 \neq 0$ corresponds to a finite ordinary viscosity ν for the odd-viscous fluid. In [21], it has been stated that for small ν, a first Chern number can still be assigned to the bands, equal by continuity to the one obtained at vanishing ordinary viscosity. There are some subtleties due to the Hamiltonian being non-Hermitian, a suggested reading is [41]. It is expected that all the phenomenology discussed in the absence of ordinary viscosity $\nu = 0$ will also occur when it ν is not strictly zero, up to an attenuation of all the waves, which might depend on the wave-vector. Then, the same expectations are addressed to the case of small passive elastic moduli B, μ_1, μ_2.

Conclusions

In this work we have studied the behaviour of an active plate with odd elasticity. We have worked within the Reissner-Mindlin theory—permitting the points along the lines perpendicular to the midplane not to end up along the lines perpendicular to the deformed midplane—and considered a plate made of an odd-elastic material with cylindrical isotropy and no internal torques.

We have found that the horizontal deformations of the midplane are decoupled from the flexural deformations of the plate; the former are described by 2D odd elasticity, while the latter are described by three coupled differential equations, which show new phenomena. The plate has three independent cycles of deformation that extract energy from the system: in addition to the one obtained deforming horizontally the midplane (already identified in 2D odd elasticity), we have two cycles that regard the flexural dynamics: one is analogous to the planar cycle, as it involves the same shear components—as well as the same odd modulus K_1^o—but has a different distribution across the thickness of the plate; the other consists in a rotation of the vector $\boldsymbol{\phi}$ and extracts an energy amount proportional to K_2^o.

Then, we have focused on the flexural dynamics, discovering that the band-system becomes gapped for increasing activity. The analytical study of the topological properties has been performed in the simplified case of a pure active plate, i.e. setting all the passive elastic moduli to zero. When both the active moduli are non-zero, the momentum space can be compactified to a sphere, allowing a well defined Chern number. We have found that the Chern number is equal to two when the odd moduli have opposite signs, and vanishes otherwise. We have then estimated the profile shape and the penetration depth of the edge modes. Finally, we have provided an exact mapping of the flexural dynamics with non-zero μ_1, K_1^o, K_2^o onto the odd-viscous model. This has allowed us to adapt the simulations performed in [21] to our system. The simulations show that, as long as the topological invariant is non-zero, the edge modes propagate unidirectionally and do not backscatter when encounter obstacles; while they propagate in both the directions and do backscattering when topological protection is absent.

References

1. Ramaswamy, S. Active matter. *Journal of Statistical Mechanics: Theory and Experiment* **2017,** 054002 (2017).
2. Shankar, S., Souslov, A., Bowick, M. J., Marchetti, M. C. & Vitelli, V. *Topological active matter* 2021.
3. Marchetti, M. C. *et al.* Hydrodynamics of soft active matter. *Rev. Mod. Phys.* **85,** 1143–1189 (2013).
4. Polygerinos, P. *et al.* Soft Robotics: Review of Fluid-Driven Intrinsically Soft Devices; Manufacturing, Sensing, Control, and Applications in Human-Robot Interaction. *Advanced Engineering Materials* **19,** 1700016 (2017).
5. Ramaswamy, S. The Mechanics and Statistics of Active Matter. *Annual Review of Condensed Matter Physics* **1,** 323–345 (2010).
6. Fruchart, M., Hanai, R., Littlewood, P. B. & Vitelli, V. Non-reciprocal phase transitions. *Nature* **592,** 363–369 (2021).
7. Needleman, D. & Dogic, Z. Active matter at the interface between materials science and cell biology. *Nature Reviews Materials* **2,** 17048 (2017).
8. Soni, V. *et al.* The odd free surface flows of a colloidal chiral fluid. *Nature Physics* **15,** 1188–1194 (2019).
9. Salbreux, G. & Jülicher, F. Mechanics of active surfaces. *Phys. Rev. E* **96,** 032404 (2017).
10. Banerjee, D., Souslov, A., Abanov, A. G. & Vitelli, V. Odd viscosity in chiral active fluids. *Nature Communications* **8,** 1573 (2017).
11. Brandenbourger, M., Locsin, X., Lerner, E. & Coulais, C. Non-reciprocal robotic metamaterials. *Nature Communications* **10,** 4608 (2019).
12. Scheibner, C. *et al.* Odd elasticity. *Nature Physics* **16,** 475–480 (2020).
13. Chen, Y., Li, X., Scheibner, C., Vitelli, V. & Huang, G. *Realization of active metamaterials with odd micropolar elasticity* 2021.
14. Tan, T. H. *et al. Development drives dynamics of living chiral crystals* 2021.
15. Hasan, M. Z. & Kane, C. L. Colloquium: Topological insulators. *Rev. Mod. Phys.* **82,** 3045–3067 (2010).

16. Ozawa, T. *et al.* Topological photonics. *Reviews of Modern Physics* **91,** 015006 (2019).

17. Zhang, X., Xiao, M., Cheng, Y., Lu, M.-H. & Christensen, J. Topological sound. *Communications Physics* **1,** 97 (2018).

18. Huber, S. D. Topological mechanics. *Nature Physics* **12,** 621–623 (2016).

19. Souslov, A., van Zuiden, B. C., Bartolo, D. & Vitelli, V. Topological sound in active-liquid metamaterials. *Nature Physics* **13,** 1091 (2017).

20. Shankar, S., Bowick, M. J. & Marchetti, M. C. Topological Sound and Flocking on Curved Surfaces. *Phys. Rev. X* **7,** 031039 (2017).

21. Souslov, A., Dasbiswas, K., Fruchart, M., Vaikuntanathan, S. & Vitelli, V. Topological Waves in Fluids with Odd Viscosity. *Physical Review Letters* **122,** 128001 (2019).

22. Delplace, P., Marston, J. B. & Venaille, A. Topological origin of equatorial waves. *Science* **358,** 1075–1077 (2017).

23. Landau, L. *et al. Theory of Elasticity* (Elsevier Science, 1986).

24. Marsden, J. E. & Hughes, T. J. *Mathematical foundations of elasticity* (Courier Corporation, 1994).

25. Fruchart, M. & Vitelli, V. Symmetries and Dualities in the Theory of Elasticity. *Phys. Rev. Lett.* **124,** 248001 (2020).

26. Nakahara, M. *Geometry, Topology and Physics* (CRC press, 2003).

27. Fruchart, M. & Carpentier, D. An introduction to topological insulators. *Comptes Rendus Physique* **14,** 779–815 (2013).

28. Klitzing, K. v., Dorda, G. & Pepper, M. New Method for High-Accuracy Determination of the Fine-Structure Constant Based on Quantized Hall Resistance. *Physical Review Letters* **45,** 494–497 (1980).

29. Halperin, B. I. Quantized Hall conductance, current-carrying edge states, and the existence of extended states in a two-dimensional disordered potential. *Physical Review B* **25,** 2185–2190 (1982).

30. Thouless, D. J., Kohmoto, M., Nightingale, M. P. & den Nijs, M. Quantized Hall Conductance in a Two-Dimensional Periodic Potential. *Physical Review Letters* **49,** 405–408 (1982).

31. Simon, B. Holonomy, the Quantum Adiabatic Theorem, and Berry's Phase. *Physical Review Letters* **51,** 2167–2170 (1983).

32. Haldane, F. D. M. Model for a Quantum Hall Effect without Landau Levels: Condensed-Matter Realization of the "Parity Anomaly". *Physical Review Letters* **61,** 2015–2018 (1988).

33. Hatsugai, Y. Chern number and edge states in the integer quantum Hall effect. *Physical Review Letters* **71,** 3697–3700 (1993).

34. Haldane, F. D. M. & Raghu, S. Possible Realization of Directional Optical Waveguides in Photonic Crystals with Broken Time-Reversal Symmetry. *Physical Review Letters* **100,** 013904 (2008).

35. Prodan, E. & Prodan, C. Topological Phonon Modes and Their Role in Dynamic Instability of Microtubules. *Physical Review Letters* **103,** 248101 (2009).

36. Vitelli, V. Topological soft matter: Kagome lattices with a twist. *Proceedings of the National Academy of Sciences* **109,** 12266–12267 (2012).

37. Kane, C. L. & Lubensky, T. C. Topological boundary modes in isostatic lattices. *Nature Physics* **10,** 39–45 (2014).

38. Tauber, C., Delplace, P. & Venaille, A. Anomalous bulk-edge correspondence in continuous media. *Physical Review Research* **2,** 013147 (2020).

39. Graf, G. M., Jud, H. & Tauber, C. Topology in Shallow-Water Waves: A Violation of Bulk-Edge Correspondence. *Communications in Mathematical Physics* **383,** 731–761 (2021).

40. Reddy, J. N. *Theory and analysis of elastic plates and shells* (CRC press, 2006).

41. Shen, H., Zhen, B. & Fu, L. Topological Band Theory for Non-Hermitian Hamiltonians. *Phys. Rev. Lett.* **120,** 146402 (2018).